

**PHOTOCATALYTIC PERFORMANCE OF PHYTO-ENHANCED ZINC
OXIDE (ZnO) DOPED WITH GRAPHITIC CARBON NITRIDE (g-C₃N₄) ON
THE DEGRADATION OF SIMULATED SOLUTION OF TETRACYCLINE**

BY

**ADOGWA, Alexander Abu
MEng/SEET/2017/7345**

**DEPARTMENT OF CHEMICAL ENGINEERING
FEDERAL UNIVERSITY OF TECHNOLOGY
MINNA**

OCTOBER, 2021

ABSTRACT

Photocatalytic degradation of simulated solution of tetracycline using plant mediated (phyto-enhanced) zinc oxide doped with graphitic carbon nitride was investigated under solar light irradiation for 3 hours. Leaf extract from *Moringa oleifera* was the source of the phytochemical constituents used in the phyto-enhancement of zinc oxide synthesized by precipitation method using zinc nitrate precursor. Doping was achieved by physically mixing phyto-enhanced synthesized zinc oxide with graphitic carbon nitride, a light yellow powder gotten from the calcination of melamine at 550 °C. The produced photocatalyst was characterized by FTIR, SEM-EDX, XRD and BET to determine the functional groups, structural morphology, elemental composition, crystallinity, surface area, pore volume and pore diameter. Doped phyto-enhanced zinc oxide showed evolved morphology, revealed loosed structure of uniformly distributed particles with increased surface area. This was confirmed by BET as the surface area (346.1 m²/g) was 10 times greater than that of pure zinc oxide (35.44 m²/g). The pore diameter and volume were 5.428 nm and 0.123 cm³/g respectively compared to 2.965 nm and 0.01259 cm³/g of pure zinc oxide. FTIR spectrum was recorded in the range of 4000–500 cm⁻¹. The FTIR result showed that Zn–O functional group was found at low wavenumber. The XRD pattern of doped phyto-enhanced zinc oxide nanoparticles showed that the substances only belong to ZnO although there were diffraction peaks of other impurities as a result of surface contamination and storage. The average crystallite size of the pure zinc oxide and the doped phyto-enhanced zinc oxide was estimated to be 29.87 nm and 30.27 nm respectively using Debye Scherer equation. The effective operation parameters employed to enhance the photocatalytic process are solution pH, initial concentration and catalyst dosage. The result showed that 98.7% degradation of tetracycline concentration of 5 mg/L was obtained with the optimum doping ratio of 5% (w/w), pH 8 and photocatalyst dosage of 0.2 g/L. This may be attributed to narrow band gab and improved electron/hole separation efficiency. Based on this outcome, it can be concluded that, phyto-enhanced zinc oxide doped with graphitic carbon nitride photocatalyst can effectively degrade tetracycline in pharmaceutical effluents.

CHAPTER ONE

1.0

INTRODUCTION

1.1 Background to the Study

Antibiotics as additives have been reported to have gained wide acceptance in medicine and agriculture. This has led to enhanced growth, boost efficiency and curbing of disease outbreaks. Recently, the detection of tetracycline (TC) antibiotics in the environment is reported (Priya and Radha, 2017). This has been attributed to the unrestrained release of untreated wastewater from the pharmaceutical industries, residues from intensive farming and human excretion (Wang *et al.*, 2018a). The presence of TC in the environment has reportedly caused harmful effects leading into antibiotic opposed genes (Zhu *et al.*, 2018). Existing wastewater remediation methods such as adsorption, membrane filtration and chemical coagulation, have been reportedly deficient in TC removal (Xiong *et al.*, 2018). These methods do not mineralize organic contaminants but only transfer pollutants from one phase to another leading to secondary pollution. Hence, affordable green processes must be developed to ensure complete mineralization of pollutants (Saadati *et al.*, 2016). Recently, advanced oxidation processes (AOPs) are being suggested as the best technologies for TC removal by degradation from wastewater (Li *et al.*, 2018). AOPs are known for their rapid conversion rates with non-targeted oxidation, resulting in coexistent degradation of multiple pollutants (Krishnan *et al.*, 2017). Heterogeneous photocatalysis seems to have gained more popularity amongst the AOPs as it has been conveniently applied in the degradation of pollutants into H₂O and CO₂ (Sohrabi *et al.*, 2017) and can be carried out under ambient conditions (Lam *et al.*, 2012).

Metallic semiconductor photocatalyst such as TiO₂ and ZnO are cost-effective, reportedly efficient and environmentally-friendly materials that have been utilized for the remediation of the environment (Chen *et al.*, 2017a). Impressively, zinc oxide has an edge

over others as it is known to exhibit high effectiveness in photocatalysis. ZnO has a broad band gap of 3.37 eV at ambient condition, a high binding energy of 60 meV, optical properties, high catalytic activities and induces electron-hole pairs in the presence of UV light (Sahu *et al.*, 2017). The electron and holes can interact with the dissolved O₂ and H₂O to produce O₂[•] (superoxide radical) and OH[•] (hydroxyl radical) respectively. These radicals are responsible for the reduction and oxidation of pollutants into CO₂ and H₂O (Chen *et al.*, 2017a).

These qualities have aroused the interest of the research community to develop novel techniques for the production of ZnO through existing techniques. However, toxic chemicals are reportedly used to maintain stability. This has led to poisonous environment. In order to overcome this bottleneck, the use of plants (phyto) extract also called phyto-enhancement is suggested as it is reportedly eco-friendly, economically advantageous and offers natural stabilization (Priya and Radha, 2017). This synthesis also permits distinct morphology of nanoparticles which improves photocatalytic activities and guarantees stability. Fundamentally the known metabolites present in plant extract are saponins, tannins, starches, polypeptides, terpenoids, flavanoids and phenolics. These perform the role of reducing Zn²⁺ to Zn⁰ (Fakhari *et al.*, 2019). Although phyto-enhanced ZnO is reported to have a slightly reduced band gap, it is still not within the visible light region. Also, the frequent recombination of photo-induced holes/electrons is still a prevailing challenge seeking for attention. Therefore, to effectively produce a photocatalyst like ZnO, the best possible means to reduce the band gap and curb the photo-induced charge recombination has to be identified (Li *et al.*, 2015).

In a buildup to surmount these challenges, doping has been suggested. It is a technology which adjusts physical properties and the electronic structure of ZnO so as to improve the visible light response to radiation from the sun and ensure reduced e⁻/h⁺ recombination

(Kong *et al.*, 2017). For example, Cho *et al.*, (2010) reportedly improved the utilization of visible light by ZnO through doping with carbon sourced from vitamin C, whereas Sawant *et al.*, (2016) reportedly synthesized zinc oxide nanoparticles active in visible light region using an aniline nitrate complex. Similarly, Liang *et al.*, (2016) used 2-methylimidazole, a zinc based framework to develop a carbon rich zinc oxide responsive to visible light. Legitimately, these materials rich in carbon extended the visible light response and photocatalytic activity of ZnO (Ansari *et al.*, 2017). Regrettably, these have not satisfactorily altered the characteristics of ZnO that will make it an excellent photocatalyst.

Recently, attention has shifted towards the use of dopants such as graphitic carbon-nitride (g-C₃N₄) sourced from melamine. It is unaccustomed to but with latent potentials and enormous applicability. In this work, the use of phyto-enhanced zinc oxide doped with graphitic carbon nitrite for the complete removal of tetracycline pollutant in a synthetic pharmaceutical wastewater was investigated under sunlight irradiation. Furthermore, effect of operation parameters and kinetics of the process was also determined.

1.2 Statement of the Research Problem

Global economic growth is increasing exponentially, but at the same time, rapid urbanization and industrialization releases enormous volumes of wastewater, imposing various adverse effects on human health and causing breakdown in the quality of the environment as a whole. It has been revealed that generation of wastewaters with complex and recalcitrant molecules is increasing day by day. The presence of these organic compounds in water poses a serious threat to public health since most of them are toxic, endocrine disrupting, mutagenic, or potentially carcinogenic to humans, animals and aquatic life (Ameta *et al.*, 2018). Regrettably, about 4 billion people worldwide have little or no access to portable water while millions die annually due to the hazard of water

pollution. Even the so-called recycled wastewater has been reported to now carry health-threatening coliforms and soluble refractory organic compounds that are both expensive and tedious to treat (Chong *et al.*, 2010). Thus, the removal of these organic contaminants prior to discharge into the environment is vital. Among the advanced oxidation processes that have been widely studied, heterogeneous photocatalysis has demonstrated to be effective for degradation of both water and atmospheric organic contaminants (Hameed *et al.*, 2011). To this end, huge demand is incumbent on the scientists, environmentalists as well as the engineers to find possible methods of treating industrial effluents. Most researchers adopt photocatalysis to remove pollutants from wastewaters because of its ability to completely mineralize the target pollutant (Krishnakumar *et al.*, 2010)

1.3 Aim and Objectives of the Study

The aim of this research work is to degrade pollutants in pharmaceutical wastewater using heterogeneous photocatalysis under sunlight irradiation. This will be achieved through the following objectives:

- I. Synthesis of ZnO nanoparticles using phytochemicals from *Moringa oleifera* leaf extract and zinc nitrate hexahydrate as the precursor
- II. Doping of phyto-enhanced zinc oxide with graphitic carbon-nitrite from melamine
- III. Phytochemical analysis of the *Moringa oleifera* leaf extract
- IV. Characterization of the prepared catalyst using FTIR, SEM/EDX, XRD and BET techniques
- V. Application of the prepared catalyst on wastewater via batch photocatalysis process for the mineralization of tetracycline in wastewater with respect to the effect of concentration, solution pH, and catalyst dosage.

VI. Kinetics evaluation of tetracycline degradation on the doped phyto-enhanced photocatalyst

1.4 Justification of the Study

Various technologies for treating these harmful effluents have been developed in recent years, however Advanced Oxidation Processes (AOPs) are much suitable due to their efficiency and economic viability. Photocatalysis is known as an efficient method of treating effluents and for complete mineralization of toxic pollutants into water (H₂O) and carbon dioxide (CO₂) as opposed to the conventional methods. Green synthesis otherwise phyto-enhancement of zinc oxide (ZnO) with zinc nitrate as precursor and *moringa oleifera* leaf extract to serve as capping/reducing and stabilizing agent will certainly solve the menace of contamination and formation of hazardous by products in industrial effluents. Green synthesis is employed in this research because it is cheap, eco-friendly, and highly efficient method since it does not use toxic precursor as compared with the physical and chemical synthesis approach. No doubt, the green synthesis of (ZnO) using extract solution from *moringa oleifera* will help to increase the surface area, whereas doping will suppress electron/hole recombination and subsequently enhance the photocatalytic efficiency of zinc oxide nanoparticles (ZnONPs). ZnO is used because it is relatively cheap, stable and has high photocatalytic activities (Hameed *et al.*, 2011).

1.5 Scope of the Study

This work is limited to the preparation and characterization of phyto-enhanced zinc oxide doped with graphitic carbon-nitrite, batch process of photocatalytic degradation of simulated tetracycline solution and investigation of the optimum operating parameters.

CHAPTER TWO

2.0 LITERATURE REVIEW

2.1 Tetracycline

Tetracycline (TC) is an antibiotic widely used in the health care of both humans and animals. Although TC is a highly effective antibiotic, there has been a decline in its usage owing to arising bacteria resistance (Wang *et al.*, 2018a). Figure 2.1 shows the chemical structure of tetracycline. TC has a linear structure with fused-ring backbones (usually with heavy substitutions) a peculiar group of amide (Priya and Radha, 2017). Table 2.1 shows the functional groups present in tetracycline.

Tetracycline has been reportedly successful in the treating several kinds of bacterial and microbial infections like gonorrhoea, pneumonia, anthrax, cholera syphilis, meningitis, typhoid in human and animals, since they are active over a wide range. It has also been reported by a number of authors that it has been used for prophylaxis in handling different severe complications as leprosy, peptic ulcer, arthritis, malaria (Priya and Radha, 2017). TC is equally useful in veterinary medicine in animal husbandry to increase the effectiveness of their feeding and promote growth.

There are equally useful in fish farming, crop production, and the rearing of honey-bees, especially for the prevention of infections (Song *et al.*, 2019). TC undergoes incomplete metabolism in living organisms, leading to its excretion in active state through urine and faeces (He *et al.*, 2017).

Almost 80-90% of it could be recovered from parent's excreta in original form, this has resulted in its frequent detection in sewage discharges in amounts up to 0.1 – 1.0 microgram per liter (Ahmadi *et al.*, 2017).

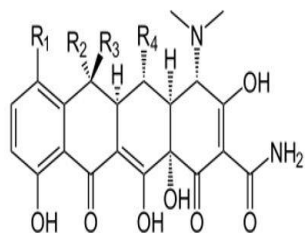


Figure 2.1: Chemical structure of Tetracycline (Saadati *et al.*, 2016).

Table 2.1: Functional groups in tetracycline

Compound	R ₁	R ₂	R ₃	R ₄
Tetracycline	H	OH	CH ₃	H
Oxytetracycline	H	OH	CH ₃	OH
Chlortetracycline	Cl	OH	CH ₃	H
Doxycycline	H	H	CH ₃	OH

TC residues detected in our surrounding is responsible for varieties of health challenges reported, these includes chronic toxicity resulting into antibiotic-resistant gene (Zhu *et al.*, 2018). TC removal has been widely studied by other researchers (Chen *et al.*, 2017). According to Xiong *et al.*, (2018), it is challenging to remove TC contaminants in wastewater due to its variable oxidation state, low biodegradability and complex structure. However, various authors have attempted to study the complete removal or degradation to harmless components, these includes; ultrasonic induced processes (Soltani *et al.*, 2016a), electro-coagulation (Ahmadi *et al.*, 2012), advance biological

methods (Aydin *et al.*, 2014), adsorption (Soltani *et al.*, 2014), photo-peroxi-coagulation (Ahmadi *et al.*, 2016), photocatalytic degradation (Soltani *et al.*, 2016b). The removal of antibiotics from wastewater in recent times have become an important research subject for the research community. This has led to many experiments being conducted with the hope of achieving remarkable success. The toxic effect of the high/low concentration of these antibiotics in our surrounding is responsible for ecological imbalance and antibiotic resistance gene. These observations indicate that the removal of antibiotics is imperative at every concentration (Nikravan, 2015).

2.2 Wastewater Treatment Methods

There are three categories of wastewater treatment methods namely: physical, biological and chemical. This is displayed schematically in Figure 2.2.

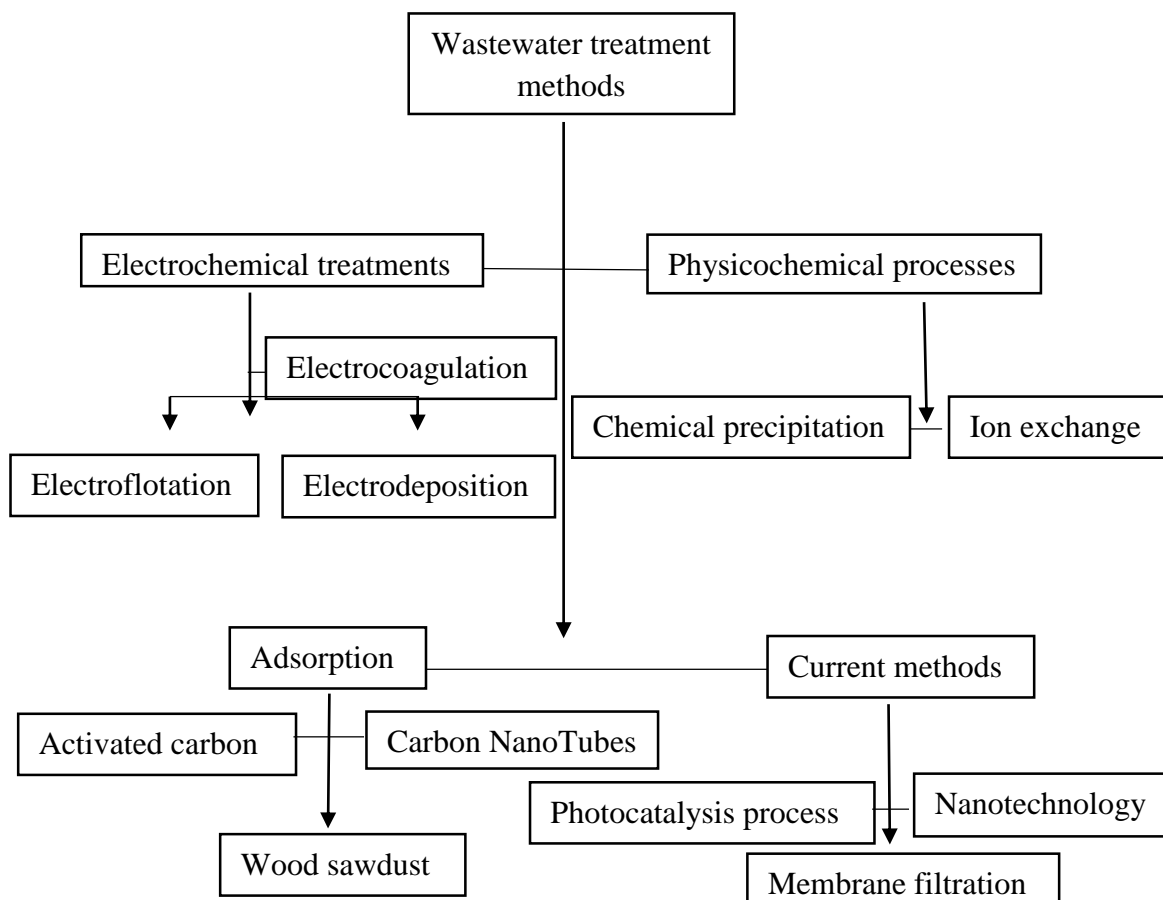


Figure 2.2: Methods of wastewater treatment (Holkar *et al.*, 2016)

2.2.1 Physical processes

Adsorption and membrane-filtration processes are some of the best known physical processes that have been universally employed in wastewater treatment. Membrane processes are reportedly not devoid of shortcomings; fouling of the membrane occurs within a short period of usage. This has resulted to their periodic replacements which is very expensive. Alternatively, adsorption method provides processes of higher efficiencies relative to the conventional physical processes, and particularly when the adsorbent used has low cost, is a waste material, and doesn't need vigorous pre-processing prior to its usage. Studies have shown that several adsorbent such as polymer materials, resins, biochar have been used with activated-carbon as high-efficiency adsorbents with numerous applications. Although, adsorption process is efficient, it is reportedly less attractive because it's difficulty in adsorbent regeneration and has high cost implication if utilized industrially (Holkar *et al.*, 2016).

2.2.2 Biological processes

In contrast to the physicochemical processes, biological method is reportedly the cheapest method used for wastewater treatment. Microorganisms such as fungi, bacteria and algae have the needed proficiency in the removal of different pollutants present in wastewater and have been used in treatments of most industrial effluents. In a detail sense, this process could be classified into anaerobic, aerobic and anoxic. Although, many organic pollutants are degraded, many others resist this process majorly because of complicated structure (Basnet *et al.*, 2018).

2.2.3 Chemical processes

Chemical processes involve the use of chemical reagents in the process of degradation, transformation or oxidation of identified pollutants completely. These processes include, flocculation, electroflotation, coagulation electrokinetic coagulation, oxidation methods

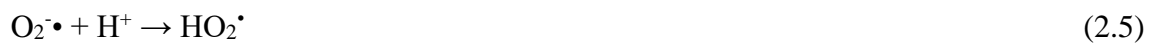
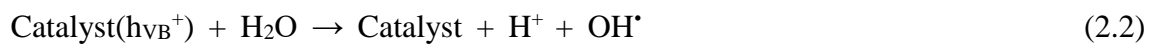
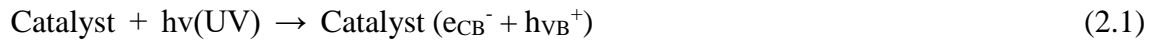
(Holkar *et al.*, 2016). In recent times, report shows that chemical methods are often considered one of the best methods for decoloration of wastewater. The most employed amongst these processes for degradation is the oxidation process due to the easy in operation. Chemical processes are mainly chemical oxidation and advance oxidation processes (AOPs). These two categories have the competence to mineralize organic pollutants completely, degrade pesticides and other common pollutants either partly or completely under ambient conditions. The AOPs can also be further divided thus; photocatalytic oxidation (in the presence of either UV irradiation or sunlight for catalyst activation) and Fenton chemistry. These have demonstrated their ability to treat effluents containing recalcitrant pollutants (Holkar *et al.*, 2016).

Most wastewater treatment technologies that have been attempted includes; chlorination, coagulation and adsorption have known record of transferring pollutants from one phase to another rather than degrading them completely. This result in a secondary pollution whereas processes like filtration, sedimentation, membrane and chemical technologies incurs expensive cost operation and have high risk of breeding other contaminants. These have generated curiosity amongst research community which have led to many researches in the field of AOPs with the aim of improving the outcome of wastewater remediation. Amongst the AOPs, heterogeneous photocatalysis is the current trend (Satyawali and Balakrishnan, 2008).

2.3 Photocatalysis

Photocatalysis refers to a photo-induced reaction of a catalyst exposed to UV or sunlight irradiation. This reaction can be initiated when photons are absorbed with adequate energy that is sufficient/greater than bandgap energy of photocatalyst in use. Consequently, this action results in the separation of charges due to the release of an electron from the valance to the conduction band of the catalyst, hence creating a hole

(h^+) in the valence band. For any photocatalytic reaction to be favored, recombination must be prohibited as much as possible (Hammed *et al.*, 2011). According to Akpan and Hammed (2009), the process of pollutant degradation by a photocatalyst exposed to UV irradiation can be expressed by the Equations below; and the reaction mechanism as proposed by Ani *et al.*, (2018) is presented in figure 2.3.



TC

Where $h\nu$ is the photon, V_B is the valence band, C_B is the conduction band, OH^* is hydroxyl radical, $\text{O}_2^{\bullet-}$ is superoxide radical.

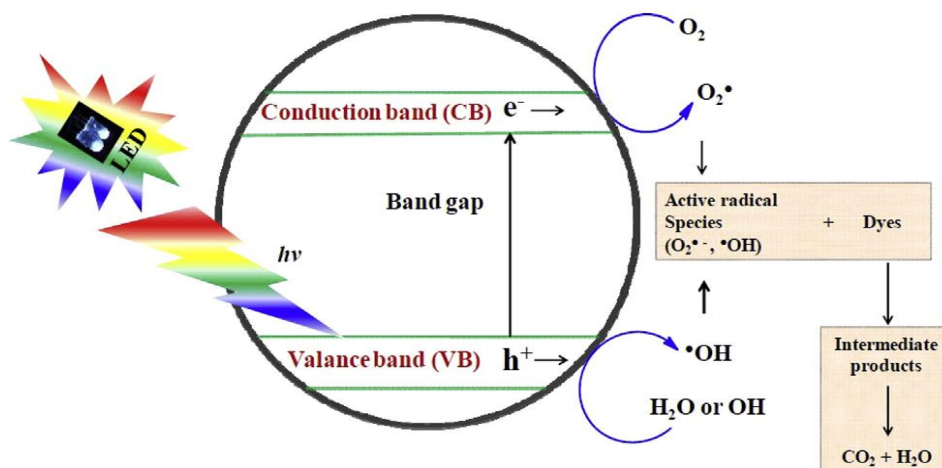


Figure 2.3: Reaction Mechanisms for Zinc Oxide (ZnO) Photocatalyst (Ani *et al.*, 2018)

2.4 Basic Properties of Good Photocatalyst

Ahmed *et al.*, (2017) reported that ZnO nanoparticles (NPs) can exist in solid phase or as a liquid suspension. Regardless of the phases involved, a number of factors are considered for a catalyst to be regarded as a good photocatalyst. These include;

- a) High surface area
- b) Good photo-stability
- c) Appropriate band gap
- d) High carrier mobility
- e) Correct band-edge positions
- f) Efficient light absorption

Also, the author justified the use of photocatalysis in wastewater degradation due to the following reasons:

- a) Active species
- b) Reactions take place at room temperature and pressure
- c) Re-use of photocatalyst is guaranteed
- d) No need for post processes
- e) No consumption of expensive oxidizing chemicals
- f) Applicable to both slurry and immobilized reactors
- g) Regeneration prospect (Ahmed *et al.*, 2017)

2.5 Zinc Oxide (ZnO) Photocatalyst

ZnO is widely acclaimed to have a bandgap of 3.21 eV (Ajala *et al.*, 2018) with a high binding energy (60 meV) (Vishnukumar *et al.*, 2018). Zinc oxide (ZnO) is recently considered to be among the most significant binary II–VI compounds with wurtzite structure (Byzynski *et al.*, 2017). It is reported to have the attention of researchers owing to its exceptional properties and multipurpose applications in diodes (Wang *et al.*, 2015),

solar cells (Lupan *et al.*, 2010), transparent conducting electrodes (Mhamdi *et al.*, 2015), gas sensors (Biasotto *et al.*, 2014), laser diodes and thin film transistor (Meshram *et al.*, 2011; Wang *et al.*, 2018b). Different methods have successfully produced ZnO thin film such as spray pyrolysis, RF sputtering, sol–gel method amongst others (Ibrahim *et al.*, 2013). As an alternative to TiO₂, ZnO has been reported as an effective catalyst, although researches have also been conducted using ZrO₂, SrO₂ and CdS. ZnO as reported by Wang *et al.*, (2018b) possesses unique properties that is relevant in several applications, notable among the are solar cells, transparent conducting films, ultraviolet lasers, and photocatalyst. It has recently been reported that micrometer-sized hollow structures of zinc oxide (ZnO) have enticed majority of researchers as photocatalysts because of their low cost, applicable flat band potential high electron mobility, environmental friendliness as well as environmental sustainability (Wang *et al.*, 2017).

2.5.1 ZnO structure

According to Lee *et al.*, (2015), ZnO has a well-defined crystal wurtzite or cubic (zinc blende) structures which are normally in rock salt. The rock salt structure of ZnO is produced at intense pressure making its structure uncommon. Thermodynamically, of the three structures, wurtzite structure of ZnO which is the most common has the best stability. ZnO crystal structure is hexagonal wurtzite at ambient temperature and pressure, having two lattice constants values approximately 0.3 nm and 0.5 nm (Baruah and Dutta, 2009). Figure 2.4, exhibits the structures of ZnO; it can be detected that the wurtzite ZnO contains atoms developing hexagonal-close pack sub-lattices which will stack alternatively along the *c*-axis. When situations of this kind occur, it will be observed that each Zn²⁺ sub-lattice contains four Zn²⁺ ions and surrounded by four O₂⁻ ions and vice versa, coordinated at the edges of a tetrahedron. Similarly, the tetrahedral coordination produces polar symmetry along the hexagonal axis. This polar symmetry creates

spontaneous polarization which is an important parameter affecting ZnO crystal growth in the cause of synthesis.

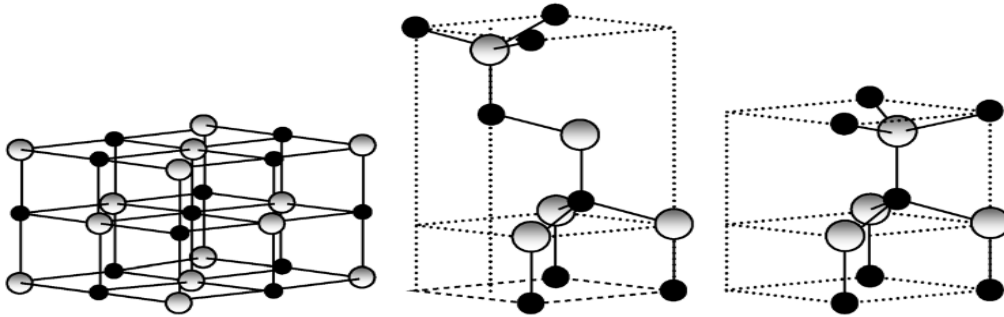


Figure 2.4: ZnO crystal structures from left to right (a) cubic rocksalt; (b) cubic zincblende; (c) hexagonal wurtzite. The larger and smaller spheres denote Zn and O atoms respectively (Lam *et al.*, 2012).

2.5.2 Challenges of ZnO as a photocatalyst

Researchers in photocatalysis ultimately desires at all times to design as well as to fabricate photocatalyst that possesses suitable band structure, good redox potential, high photoactivity at visible region and good stability. Sadly, these are still the challenging practices in the world of photocatalyst synthesis and activity. It is also true that in the conventional processes, the inadequate solution to recombination and/or the inability to absorb light rays in the visible region are inevitable problems associated with photocatalysis. Nevertheless, much efforts have been devoted to bringing these limitations to check. Remarkably and irrespective of its resourcefulness, ZnO photocatalyst is still not devoid of challenges. Most notable amongst these challenges are explained as follows (Wang *et al.*, 2017, Samadi *et al.*, 2016, Kumar *et al.*, 2017, Pirhashemi, *et al.*, 2018):

(a) The ineffectiveness of ZnO photocatalyst is because of the characteristic broad band gap. As a result, the catalyst can only absorb limited portion of the energy beam from the sun (3–5%).

(b) ZnO photocatalyst is also known for the spontaneous recombination of the photo-induced charge carriers which limits them from getting to the surface, thereby resulting in reduction of the reactions that are known to occur on the liquid interface/semiconductor; and

(c) ZnO photocatalyst is highly rated in terms of photo-corrosion when exposed to irradiation. Furthermore, ZnO dissolves in acidic and alkaline solutions; though reactions are favored in the later.

Consequently, pure ZnO photocatalyst have not been able to meet up to the projection of researchers on photoactivity under natural sunlight. To this end, extensive researches have been geared up to improving photo-catalytic activity of ZnO by overcoming the known drawbacks encountered as photocatalyst. Interestingly, several researches are currently working on how to improve the visible light response of ZnO based photocatalyst by applying techniques like: creation of hetero-junctions between semiconductors, band gap narrowing through the integration of ZnO with metal/non-metal dopants, amongst others. Numerous insightful and useful researches on the analysis of these strategies are documented reported extensively (Pirhashemi, *et al.*, 2018; Selvin *et al.*, 2017; Adhikari *et al.*, 2014; Anirudhan and Deepa, 2017).

2.5.3 Strategies to improve the photodegradation efficiency of ZnO

The major obstacle commonly associated with photocatalysis is the inability to withstand for long the charge separations of photogenerated hole ($h\nu B^+$) and electron (eCB^-). This recombination step causes energy wasting and lowers the quantum yield. To remove this

setback, the e^-/h^+ recombination must be subdued to guarantee effective photocatalysis. The use of dopants could solve the problem of recombination by introducing barriers for the electrons and holes to remain separate. Subsequently, the dopants may hinder electrons thereby decreasing the chances of electron-hole combining again. In addition, intermediate species like hydroxyl and superoxide radicals generated will highly improve the charge separation efficiency. On a wider note, nature and dopant ratio, operating parameters and synthesis method significantly affect the photo-effectiveness of doped photocatalyst (Lee *et al.*, 2015).

2.6 Phyto-enhanced Synthesis

Conventional techniques such as physical and chemical methods have been employed over the years in the production of ZnO nanoparticles. These methods include; sol-gel combustion, chemical vapor deposition, microwave assisted, precipitation, sonochemical, hydrothermal, wet polymerization, solvothermal, thermal decomposition (Matinise *et al.*, 2017). But these methods are reportedly toxic, have high energy requirement and potentially hazardous. Being aware of this, the development of an alternative that is reliable, biocompatible, environmentally friendly and economically viable has become imperative as reported by Keong *et al.*, (2017). Biosynthesis of nanoparticles involves reduction/oxidation. The plant phytochemicals are responsible for the oxidation/reduction reactions in the preparation of ZnO oxide nanoparticles. The three major choices that must be made for an ecofriendly synthesis evaluated from green perspective includes: Solvent medium, reducing and stabilization agent (Kaur *et al.*, 2019). The phytochemical constituent of plant extract performs the role of stabilization as capping agents through different mechanisms. This is important for its functions and its subsequent applications. Basically, phytochemicals constituents reported to be in plant extracts are; saponins,

tannins, polypeptides, terpenoids, and flavonoids. Water is used majorly as solvent for their extraction (Kalpana *et al.*, 2018).

Plant components such as roots, leaves, stems, seeds and fruits have been reportedly used for ZnO synthesis. Table 2.2 presents a summary of the synthesis of ZnO nanoparticles by several plant extracts.

Table 2.2: Synthesis of ZnO nanoparticles by extracts from plant (Zhu *et al.*, 2019)

Extracts	Zinc precursor	Size	Shape
Aloe vera	Zinc sulfate	TEM (8–18), XRD (15)	Hexagonal
Azadirachta indica	Zinc nitrate	18 (XRD)	Spherical
Calotropis gigantean	Zinc acetate	8–12 (XRD)	Spherical
Carica papaya milk	Zinc nitrate	11–26 (XRD)	Nanoflower
Coffee	Zinc acetate	4.6 (XRD)	-
Citrus aurantifolia	Zinc acetate	50–200(FESEM)	Spherical
Corymbia citriodora	Zinc nitrate	120 (TEM), 21 (XRD)	Polyhedron
Euphorbia jatropha	Zinc nitrate	50-200 (TEM)	Hexagonal
Moringa oleifera,	Zinc nitrate	16–31.9 (HRTEM)	Spherical
Plectranthus amboinicus	Zinc nitrate	C20–50 (TEM)	Spherical
Polygala tenuifolia	Zinc nitrate	33–73 (TEM)	Spherical
Solanum nigrum	Zinc nitrate	20–30 (XRD), 29.79(TEM)	Hexagonal

Additionally, due to its excellent physicochemical characteristics, ZnO photocatalyst is currently trending as viable solution to wastewater treatment remediation. Recently, the research community have proven photocatalysis has the capacity to eliminate pollutants from wastewater. Table 2.3 presents the photocatalytic application of phyto-enhanced ZnO nanoparticles synthesized used in the degradation of various pollutants.

Table 2.3: Photocatalytic application of phyto-enhanced ZnO nanoparticles synthesized for the removal of various contaminants (Zhu *et al.*, 2019; Chemingui *et al.*, 2019; Khosravi *et al.*, 2019)

Plants extract	Pollutants	Time (min)	Degradation (%)
Corymbia citriodora	Methylene blue	90	84
Citrus paradise	Methylene blue	540	56
Plectranthus amboinicus	Methylene blue	180	92.45
Eucalyptus globulus	Methyl orange	60	97
Artrocarpus heterophyllus	Rose bendel dye	120	80

U. lactuca	Methylene blue	120	90
Laurus Nobilis	Textile dye	60	90
Thymus vulgaris	Chromium	15	83

2.7 Doping Technology

The development of an effective heterogeneous photocatalyst has witnessed renewed interest in recent times. As part of the efforts by researchers to improve the photoactivity of a photocatalyst, doping has been suggested (Lam *et al.*, 2012). Semiconductors are generally characterized by energy gap. This gap in energy refers to the permissible energy needed for charging electrons impaled in a quantum state to be dissociated to partake in conduction. In a simple term, bandgap accounts for the energy differential of valence and conduction band. Hence the narrower this difference, the wider the spectral and the better the visible light response (Saadati *et al.*, 2016).

Doping is a technique that imputes trace impurities which serves as inhibitors to electron/hole recombination during irradiation. These impurities when incorporated into photocatalyst resulting in improved photo activity (Lam *et al.*, 2012). Doping of ZnO with metal ion has been widely considered. It is considered as a feasible way of enhancing the visible light-reaction of ZnO. Metal dopants in some cases are attributed to the scavenging of generated holes/electrons with improved charge carrier lifetime resulting in the inhibition of possible recombination (Saadati *et al.*, 2016).

However, reports of reduced photo response with metal dopants have been published. It has also been reported that photoactivity of ZnO doped with metals is largely dependent on few parameters namely; choice of metal ion, synthesis procedure and condition of operation. Moreover, there exists an optimum concentration of dopant, above which a negative photoactivity is expected. It has been reported that metals ions such as Na, Ag, Fe, Cr, V, La, Co, Ta and Sn improved photoactivity, whereas Pt, Cu and Mn had opposite

consequences. This varying effects is as a result of the ability of the dopants to trap and hinder electron/hole transfer and recombination (Saadati *et al.*, 2016).

The photocatalytic degradation rate of ZnO doped Sn was studied by Sun *et al.*, (2011). It was reported that methylene blue was degraded most by the doped ZnO under sunlight. With doped ZnO, methylene blue degradation was successful after 6 hours with approximately 100% COD and TOC removal after 10 hours. Whereas, pure ZnO had 87%, 48% and 71% degradation, COD and TOC removal respectively after 10 hours. Recently, non-metals such as carbon (C) and nitrogen (N) have been used as dopants for improving the photoactivity of ZnO photocatalyst under sunlight.

In contrast to metals, non-metal ions are less probable to setup recombination centers making them viable alternatives to increase photoactivity. Amongst these non-metals doped ZnO, carbon doping has been reported as the best. This is as a result of the substitution of carbon into the ZnO matrix which necessitated a shift of the valence band edge to a higher energy level consequently narrowing the bandgap. Liu *et al.*, (2011) studied under visible light irradiation, the photodegradation of RhB by C-doped ZnO. It was opined that the photocatalyst showed strong response in UV–vis ranges. This the authors suggested that it was as a result of carbon taking the position of oxygen in the catalyst and also the large surface area of the photocatalyst, enabling more active sites for photodegradation of the adsorbed pollutant.

2.8 Effects of Reaction Parameters in Photocatalysis

2.8.1 Concentration of pollutant

Pollutant concentration plays a paramount role in its degradation. If initial organic concentration is high, the tendency at which the organic molecule “binds” itself to the photocatalyst surface and “closes” the active site that leads to hydroxyl radical production

will increase and, hence lessen photocatalytic activities of the photocatalyst (Hameed *et al.*, 2011)

Anju *et al.* (2012) reported the sonophotocatalysis removal of phenol using Zinc oxide. In the authors' view, the rate of degradation increased initially as the initial concentration increases followed by constant degradation rate at higher concentration. Ye *et al.* (2015) studied the photoactivity of immobilized ZnO nanosheet in the degradation of phenol. He reported the importance of pollutant concentration in the process performance. The author noted that as concentration was increasing from 10 to 60 mg/L, the removal rate was decreasing and after 240 min, only 88.5% removal was achieved with the initial concentration of 10 mg/L. This they concluded was as a result of the high concentration of the pollutant which was greater than the hydroxyl radicals generated in the solution. This was similar to the report of Patil and Raut, (2012), Hameed *et al.*, (2011)

2.8.2 Catalyst loading

Catalyst loading effect in photodegradation of pollutants have been reported. Research has shown that degradations in photocatalysis is marked with a linear relationship between catalyst concentration and initial reaction rate (Akpan and Hameed, 2009; Patil and Raut, 2012; Diya'uddeen *et al.*, 2011). Akpan and Hameed, (2009) claimed that any increase in amount of a photocatalyst results in similar rise in the rate of degradation of pollutants. Diya'uddeen *et al.* (2011) reported similar observation in the degradation of cyanosine with varying TiO₂ dosage between 0.01 and 0.08 g/L. The study shows that greater catalyst concentrations resulted in a tremendous increase of active sites available for adsorption. Conversely, increasing the concentration beyond what is required, do not result in a substantial variation in degradation efficiency. This is because excess catalyst acts as blockage to the photon penetration. Several reviews reported a negative degradation of organic pollutants when catalyst concentration is above certain limit. This

is in agreement with reports from Patil and Raut, (2012); Akpan and Hameed, (2009); Thennarasu and Sivasamy, (2015).

Hammed *et al.*; (2011), used ZnO to degrade dye and observed that acid dye degradation increased as more catalyst was added; this is due to the incremental rise in active sites. However, over loading alternatively will hinder the rate of degradation because the excess catalysts may reduce light penetration as a result of screening effect and therefore decrease the photoactivity of the catalyst in use (Akpan and Hameed, 2009). Consequently, it is paramount to determine optimum catalyst dosage in any photocatalytic reaction.

Khan *et al.*; (2014), studied the degradation of pollutants in refinery wastewater using zinc oxide and titanium dioxide. The study revealed that degradation was on a rise till 1.2 g/L TiO₂ dosed, thereafter, the degradation decreased. Interestingly, degradation with ZnO followed a similar pattern until 0.8 g/L after which there was a decrease. This will graphically give a linear regression which implies that degradation has a direct relationship with catalyst loading. This is in agreement with the report of Patil and Raut, (2012). Scrutinizing their findings among several causes for deviation from linearity at high loading, the obvious presumption is the turbidity emanating from more than enough catalyst particles causing unnecessary cloudiness of the wastewater. It can therefore, be presumed that the absorption of UV light by the photocatalyst surface is restricted within the photocatalytic reactor Abdollahi *et al.*; (2012). 1.2 and 0.8 g/L were the optimum concentration of TiO₂ and ZnO respectively in their investigation; which is by far, less than what was reported by Diya'uddeen *et al.*; (2011) and Ye *et al.*; (2015)

2.8.3 Effect of initial pH

Several scholars have reported that pH affects the surface adsorption ability of pollutants on photocatalyst, which is important for the photocatalytic removal of pollutants (Ye *et al.*, 2015; Meshram *et al.*, 2011; Khan *et al.*, 2014; Anju *et al.*, 2012; Diya'uddeen *et al.*, 2011; Akpan and Hameed, 2009; Abdollahi *et al.*, 2012)

Ye *et al.*, (2015) observed that under extremely high acidic/alkaline condition, phenol removal was significantly low. Their investigation on the effect of varying initial pH (5 to 9) on phenol removal shows removal of phenol under UV light radiation appeared to favour the neutral solution, while lower photocatalytic degradation was noticed at either alkaline or acidic medium. (Thennarasu and Sivasamy, 2015; Chong *et al.*, 2010) have reported the same trend.

In another literature, Anju *et al.*, (2012) reported that the extent of UV-catalyzed removal of organics is observed to be reliant on the solution pH. Furthermore, it was noted that the surface properties of the photocatalyst such as band edge position, surface charge and aggregation size was highly influenced by the solution pH. Observations reveal also that degradation rate of organics is high when more targeted molecules are adsorbed successfully to the catalyst surface. This is largely dependent on the acidic/basic nature of the catalyst surface or modified surface as a result of change in solution pH (Meshram *et al.*, 2011; Khan *et al.*, 2014; Anju *et al.*, 2012).

Research shows that the pH of solution affects the catalyst surface by protonation or deprotonation process (Khan *et al.*, 2014; Akpan and Hameed, 2009; Diya'uddeen *et al.*, 2011). The report of Diya'uddeen *et al.*, (2011) and Akpan and Hameed, (2009) described the protonation or de-protonation surface of titania according to the Equations (2.9) and (2.10).



In addition, the study showed a similar effect of effluent pH on TiO₂ surface, from which they proposed the creation of three (3) different species to justify the disparities of the behaviour of the catalyst with pH. TiOH, TiOH²⁺ and TiO⁻ are the suggested species. At the amphoteric surface, Equations (2.11) and (2.12) are established owing to the acid–base equilibria dependent on the reaction medium pH as well as the point-of-zero charge (pHpzc) of the catalyst used.



Meshram *et al.*, (2011), used ZnO–bentonite nanocomposite as photocatalyst to study the degradation of phenol in a continuous flow photocatalytic reactor. They observed that adsorption capacity of organic reactant on photocatalyst is a vital factor when it comes to degradation rate in photocatalytic oxidation process. The study also revealed possible reasons for the successful degradation of phenol attributed to basic medium over acidic medium. Their observations were attributed to two phenomena:

- I. Under acidic state – protonation of the active sites which resulted in high adsorption of phenol was due to the charge on ZnO and clay. However, this resulted in a negative outcome as it hindered removal (<5% at pH 2 after 10 min).
- II. Two changes influenced by high pH occur concurrently with phenol and the nanocomposite with clay taking up an alkaline nature and consequently increasing the adsorption capacity whereas the nano-sized ZnO experiences surface modification leading to negatively charged species formation. The two features are responsible for cooperative action of concurrent adsorption trailed by photo

degradation of phenol on the nanocomposite surface. Second, phenol experiences deprotonation in a highly alkaline state which further enhanced the rate of adsorption on the nanocomposite. Hence, after a space of 10 min, nearly 66% of phenol was removed at pH level of 12 which suggests the prevalence of second phenomenon concerning the phenol degradation.

CHAPTER THREE

3.0 MATERIALS AND METHODS

3.1 Materials

3.1.1 List of chemical reagents and equipment

The chemical precursors for the synthesis of zinc oxide and graphitic carbon nitride were zinc nitrate hexahydrate $[\text{Zn}(\text{NO}_3)_2 \cdot 6\text{H}_2\text{O}]$ and melamine respectively. Tetracycline hydrochloride ($\text{C}_{22}\text{H}_{25}\text{N}_2\text{O}_8\text{Cl}$ MW:444.43 gmol^{-1}) was the model pollutant used to assess the photocatalytic effectiveness of the synthesized phyto-enhanced zinc oxide. NaOH and HCl were used for pH adjustment. There were all analytical grades (AR) as supplied and utilized without any additional purification. Table 3.1 and 3.2 shows the list of chemical reagents and list of analytical equipment respectively.

Table 3.1 List of Chemical Reagents

Chemical	Purity (%)	Supplier
Zinc nitrate hexahydrate	99.0	Sigma Aldrich
Tetracycline hydrochloride	98.0	Sigma Aldrich
Sodium hydroxide	97.0	Sigma Aldrich
Hydrochloric Acid	37.0	Sigma Aldrich

Table 3.2 List of Analytical Equipment

Equipment	Model	Location
SEM/EDX	Zeiss Auriga	University of Western Cape, South Africa
XRD	Bruker AxSD8 Cu-K radiation	Themba Laboratory Cape town, South Africa
UV-Spec	Shimadzu UV-180.	STEP-B, FUT-MINNA, Nigeria
BET	NOVA 2400e	STEP-B, FUTMINNA,
FT-IR	FT-IR Spectra machine	University of Ilorin, Nigeria

3.2 Methods

3.2.1 *Moringa oleifera* leaf sample collection and pretreatment

Moringa oleifera leaves were collected from Tudun Fulani, Bosso Local Government Area, Minna, Niger State, Nigeria. The collected leaves were gently washed with distilled water, sundried for seven (7) days and afterward was stored for subsequent usage.

3.2.2 Preparation of leaves extract

Thirty grams of the dried *Moringa Oleifera* leaf was weighed into a beaker and de-ionized water of 300 ml was poured into the beaker. The mixture was heated for 15 min at 60 °C on a heating mantle, allowed to cool at room temperature and filtered. The obtained filtrate was kept at 4 °C in a refrigerator for further use.

3.3 Synthesis of Zinc Oxide (ZnO)

The preparation of one molar (1M) concentration of sodium hydroxide (NaOH) was done by adding 40 g of the crystals into 1000 ml of de-ionized water. To synthesize ZnO, 0.7M of the zinc nitrate $[Zn(NO_3)_2 \cdot 6H_2O]$ solution was prepared by adding 20.825g of the precursor to 100 ml de-ionized water in a beaker and stirred continuously at 50 rpm for 1 h. The pH was put to 12 with the prepared 1M NaOH. 20 ml of de-ionized water was subsequently added, stirred rigorously and the precipitate formed was allowed to settle for thirty (30) min and then decanted after which the same volume of water was continually added three times and decanted respectively. The gel obtained were properly

dried in an electrically heated oven over the night at 100 °C and then calcined for 2 h in a muffle furnace set at 350 °C, cooled and stored for use.

3.4 Phyto-enhanced Synthesis of Zinc Oxide (ZnO)

30 ml of *moringa oleifera* leave extract was added to 0.7M of Zinc nitrate [Zn(NO₃)₂.6H₂O] solution and stirred for 1 h at 50 rpm. The mixture pH was subsequently adjusted to 12 with the prepared aqueous NaOH. 20 ml of de-ionized water was subsequently added, shaken rigorously and allowed to settled for thirty (30) min. The supernatant was decanted after which the same volume of water was continually added three times and decanted respectively. The gel obtained were properly dried in electrically heated oven over night at 50 °C. Thereafter it was calcined at 350 °C for 2 h in muffle furnace, cooled and stored for use.

3.5 Quantitative Determination of the Phyto-Constituents of *Moringa oleifera* Leave Extract

3.5.1. Determination of total phenols

The Folin-Ciocalteau method as outlined by (Cicco *et al.*, 2009) was employed in the quantifying the total phenolic content. Different concentrations ranging from 0.2-1.0 mg/cm³ of gallic acid and methanol extract of *moringa oleifera* leave extracts were prepared in methanol. Thereafter, 4.5 cm³ of de-ionized water was added to 0.5 cm³ of the extract and mixed with 0.5 cm³ of a ten-fold diluted Folin-Ciocalteau reagent. Five milliliters of 7.5% sodium carbonate were then added to the tubes with another 2 cm³ of de-ionized water. The mixture was let still for a duration of 90 min at room condition consequent to the absorbance measurement at 765 nm using shimadzu UV spectrophotometer (UV-1800, 240v). This determination was done in threefold with a positive control of gallic acid. This content was expressed as Gallic Acid Equivalent (GAE).

3.5.2. Determination of total flavonoids

The total flavonoid constituent of the *moringa oleifera* leave was conducted according to the method reported by Chang *et al.*, (2002). Approximately 0.5 cm³ of the extract was mixed with 1.5 cm³ of methanol, 0.1 cm³ of 1 M sodium acetate and 2.8 cm³ of de-ionized water and allowed for 0.5 h. The absorbance measurement was conducted at 415 nm using a double beam Shimadzu UV-visible 1800 spectrophotometer. Calibration curve for Quercetin was prepared as standard. Total flavonoid was estimated using the linear relationship (Equation 3.1);

$$Y = 1.2766x + 0.0448 \quad (3.1)$$

Where: Y =Absorbance (nm)

X= Concentration (mg/L).

3.5.3. Determination of total tannins

According to Chang *et al.*, (2002), approximately 2.0 g of the *moringa oleifera* leave extract was measured into a 50 cm³ beaker after which 20 cm³ of 50% methanol was added. The beaker enclosed with foil paper was set up in a water bath at 77-80 °C for 1 h and thereafter shaken to ensure uniform mixing. The resulting mixture was filtered using the Whatman No.1 filter paper into a volumetric flask of 100 cm³. 20 cm³ of de-ionized water, 2.5 cm³ of Folin-Denis solution and 10 cm³ of 17 % of Na₂CO₃ were added and mixed properly and left for 20 min. The absorbance measurement was observed at 760 nm using Shemadzu UV- spectrophotometer (UV- 1800, 240v). Calibration curve was prepared using tannic acid as standard. Total tannins were evaluated using the Equation 3.2.

$$Y = 0.5269x + 0.602 \quad (3.2)$$

Where Y= Absorbance (nm)

X = Concentration (mg/L).

3.6 Characterization of the Prepared Photocatalysts

The zinc oxide (ZnO) and phyto-enhanced zinc oxide synthesized were characterized using the following analytical procedures;

3.6.1 Experimental procedures for surface electron microscopy (SEM) analysis

0.05 g each of zinc oxide and phyto-enhanced zinc oxide synthesized samples was sprinkled on a carbon tape which was fixed onto an aluminum stub. The zinc oxide and phyto-enhanced zinc oxide synthesized were coated with gold-palladium (Au:Pd; 60:40) using Quorum T15OT for five (5) min preceding the analysis. The essence of this, is to prevent charging which interfere with images during analysis. To examine the morphology and elemental makeup of the samples, the Zeiss Auriga SEM couples with EDX were respectively used. The microscope ran at 5 KeV for imaging and 20 KeV detectors for EDX.

3.6.2. Experimental procedure for energy dispersive X-ray spectroscopy (EDXS) analysis

0.05 g each of zinc oxide and phyto-enhanced zinc oxide synthesized samples was sprinkled in a sample holder covered with carbon adhesive tape which was sputter-coated with Au-Pd using Quorum T15OT for 5 min to the commencement of analysis. The sputter coated samples were characterized using Zeiss Auriga SEM. The secondary electron mode was activated for imaging and a homogeneous region on the sample was identified. The microscope was operated with electron high tension (EHT) of 20 KV for EDX, the illumination angle was adjusted to 150° and then the elemental composition of the sample was determined.

3.6.3 Experimental procedure for X-ray diffraction (XRD) analysis

1 g each of the zinc oxide and phyto-enhanced zinc oxide synthesized samples was crushed into powder and then dispersed into a rectangular aluminum sample holder with the aid of a well cleaned spatula. The sample holder containing the sample was clipped into the XRD instrument. Bruker AXS Advance diffractometer with 2θ range of $5 - 75^\circ$, a step size of 0.028° , and operating at 45 KV and 40 mA was used to collect the XRD data. Monochromatic copper (Cu) $K\alpha_1$ radiation with a wavelength of 0.154nm was as the X-ray source. The mean crystallite size of the nanoparticles (D), were obtained using the Debye-Scherrer's Equation (Equation 3.3):

$$D = \frac{k\lambda}{\beta \cos\theta} \quad (3.3)$$

Where k is a Constant (k=0.89), $\lambda = 1.54060$ nm is the Cu- $K\alpha_1$ wavelength, θ is the Bragg's angle and β is the full width half maximum (FWHM) of the peak at 2θ . (Kaur *et al.*, 2019)

3.6.4. Experimental procedure for Brunner-Emmett-Teller (BET) analysis

The analysis for the surface area, pore volume and pore size distribution of the samples was determined by Brunauer - Emmett- Teller (N_2 BET) technique using a NOVA 4200e surface area and pore analyzer instrument. 100 mg each of the zinc oxide and phyto-enhanced zinc oxide synthesized photocatalyst powder was weighed and degassed by flowing N_2 at $90^\circ C$ for 1 h, and then held at $350^\circ C$ for 2 h. As the temperature was increased, water vapour was adsorbed from the surface and pores of the sample. The sample was left to cool down and weighed again. The instrument uses physical adsorption and capillary condensation of N_2 principles to obtain information about the surface area and porosity of ZnO

3.7 Doping of Zinc Oxide Photocatalyst

Melamine calcination in a furnace was carried out at 550 °C for two (2) h to obtain graphitic carbon-nitrite. A yellow powder graphitic carbon-nitrite was obtained and further purified at the same temperature for a further 1 h. A yellow powered brighter product was obtained, labelled and stored for use. Phyto-enhanced ZnO synthesized was mixed with the graphitic carbon-nitrite at 5% w/w doping ratio. 20 ml of de-ionized water was poured and the mixture was stirred for 360 min at a speed of 100 rpm. Thereafter the mixture aged overnight and subsequently oven dried at 100 °C. The dried mixture was calcined in a furnace at 350 °C and stored for use.

3.8 Blank and Control Experiment

The preparation of 10 ppm of Tetracycline wastewater was done by dissolving 10 mg of tetracycline hydrochloride in 1000 ml of deionize water

3.8.1 Adsorption process

Preliminary analysis on the tetracycline wastewater degradation was conducted in the dark with the phyto-enhanced doped zinc oxide photocatalyst amidst unceasing stirring for 3 h with a magnetic stirrer at 100 rpm. This was carried out to establish if the degradation of the tetracycline pollutant in the wastewater was controlled by adsorption.

3.8.2 Photolysis experiment

The photolysis experiment was carried out as 100 ml of tetracycline solution wastewater was subjected to sunlight alone for 3 h without photocatalyst. This was conducted to affirm if the complete removal of tetracycline pollutant in wastewater under sunlight irradiation without catalyst was due to photolysis.

3.8.3 Photocatalytic experiment

To investigate the photocatalytic ability of raw zinc oxide, phyto-enhanced zinc oxide and the phyto-enhanced zinc oxide doped with graphitic carbon nitrite, 0.2 g of the photocatalyst powder was dissolved in 100 ml of tetracycline solution and the solution

pH was adjusted to 2, 4, 6, 8, 10 and 12. The resulting mixture was set up on a magnetic stirrer and whirled for thirty (30) min in the dark before exposure to sunlight. This is to ensure that the adsorption-desorption equilibrium was reached. The mixture was continuously stirred under sunlight irradiation and the mineralization of tetracycline in the wastewater was monitored for 3 h. A test sample at regular interval of 30 min was taken from it and centrifuged. The resulting supernatant liquid was analyzed using UV spectrophotometer. The spectrum was recorded at a wavelength of 357 nm and the percentage removal was evaluated using Equation 3.4:

$$\text{percentage removal of tetracycline} = \frac{C_0 - C_t}{C_0} \times 100 \quad (3.4)$$

Where C_0 is the initial concentration of tetracycline in wastewater before sunlight irradiation, C_t is the concentration of tetracycline in wastewater after sunlight irradiation for time t i.e 0, 30, 60, 90, 120, 150 and 180 min. This procedure was repeated severally for the catalyst dosage of 0.1 – 0.5 g and initial concentration of 5 – 20 mg/L (Kaur *et al.*, 2019).

CHAPTER FOUR

4.0

RESULTS AND DISCUSSION

4.1 Phytochemical Screening of *Moringa Oleifera* Leaves Extract

Table 4.1 shows the outcome of the quantitative phytochemical screening conducted on the aqueous leaves extract of the *moringa oleifera*. The phytochemical assessment was conducted to unravel the phytochemicals present and their concentration respectively in *moringa oleifera* leaves extract. It was discovered that phenol, flavonoids, tannins, alkaloids and saponin were present in significant amount. These phytochemicals are responsible for capping and stabilizing nanomaterials. This implies that these plants

extracts behave in a similar manner with the commercial reducing agents such as citric acid, sodium borohydride (NaBH_4), lithium aluminium hydride (LiAlH_4).

Table 4.1 Phytochemical Assessment of the *Moringa Oleifera* Leaves Extract

Contents	Concentration (mg/100g)
Phenol	279.4
Flavonoid	61.4
Tannins	52.03
Alkaloids	12.2
Saponins	104.1

4.2 Preliminary Studies on the Degradation of Tetracycline

Table 4.2 shows the result of preliminary studies on the degradation of tetracycline at initial pollutant concentration of 10 mg/L for 180 min. It was observed that photolysis in the absence of the photocatalyst degraded 7.2% of the pollutant. This is a reflection that the degradation of tetracycline was not controlled by photolysis reaction. Also, adsorption was carried out in the dark with a removal efficiency of 29.5%. This is an improvement when compared with photolysis. Furthermore, the effectiveness of pure zinc oxide photocatalyst in the degradation of the pollutant was experimented. It shows that 50% of the tetracycline was degraded after 180 min. Similarly, phyto-enhanced zinc oxide photocatalyst was used to degrade the pollutant and 51.7% degradation efficiency was recorded. Three (3) doping ratios were employed to determine the best doping proportion for the degradation. The phyto-enhanced zinc oxide was doped with graphitic carbon nitrite at the ratio of 1, 5 and 10% w/w respectively. The degradation efficiency recorded at the various doping ratios were 76, 87.7 and 55% respectively. This showed that 5% doping ratio gave the best performance. This is an indication that doping improved the

degradation efficiency of the photocatalyst and with the right combination of operating parameters, such as catalyst dosage, solution pH and contact time, the degradation of tetracycline could still be enhanced greatly.

Table 4.2: Results of Preliminary Studies on Tetracycline Solution Degradation

Activity	Final Concentration (mg/L)	Degradation (%)
Photolysis	9.2791	7.2
Adsorption	7.0455	29.5
ZnO	4.9958	50.0
Phyto-ZnO	4.8328	51.7
1% doped phyto-ZnO	2.3983	76.0
5% doped phyto-ZnO	1.2328	87.7
10% doped phyto-ZnO	4.4938	55.0

4.3 Characterization of the Photocatalyst

4.3.1 FTIR analysis of the photocatalyst

The synthesized ZnO and green synthesized doped ZnONPs were characterized by FTIR technique. Table 4.3 gives the summary of the peaks observed. The FTIR spectra revealed functional groups associated with all the samples investigated. Figure 4.1 presents the FTIR spectra of synthesized and green synthesized doped ZnONP in the scan range of 4000–500 cm^{-1} . The characteristic peak obtained at 3484.68 cm^{-1} in synthesized ZnO belongs to O-H group while 2761.86 cm^{-1} correspond to C-H stretching of aldehydes. The presence of C=O of carbon dioxide was revealed at peak 2426.52 cm^{-1} whereas 1788.45 cm^{-1} represents C-H bending of aromatic compounds. Furthermore, 1402.79 cm^{-1} corresponds to O-H bending of carboxylic acid while 1342.61 cm^{-1} shows O-H bending of phenol. The peak at 946.74 cm^{-1} and 834.27 cm^{-1} corresponds to O-H bend of carboxylic acid and C=C of alkanes respectively. Similarly, the FTIR spectrum for the

doped phyto-enhanced ZnO nanoparticles showed peaks at 2489.64, 1773.92, 1524.31, 1384.32, 1155.73, 1069.69, 881.33, 701.05 cm^{-1} respectively. Emphatically, the shift in peaks recorded was as a result of the introduction of graphitic carbon nitrite (g- C_3N_4) as dopant which led to some modifications during synthesis. The peaks between 1500 – 600 cm^{-1} shows the typical fingerprint region of ZnONPs. The observed peak 1524.31 cm^{-1} indicates symmetric vibration of C=O (Rajendran *et al.*, 2017).

Table 4.3: Summary of Observed Peaks from X and Y

Peaks (X)	Peaks(Y)
3484.68	2489.64
2763.87	1773.92
2426.52	1524.31
1788.45	1384.32
1402.79	1155.73
1342.61	1069.69
946.74	881.33
834.27	701.05

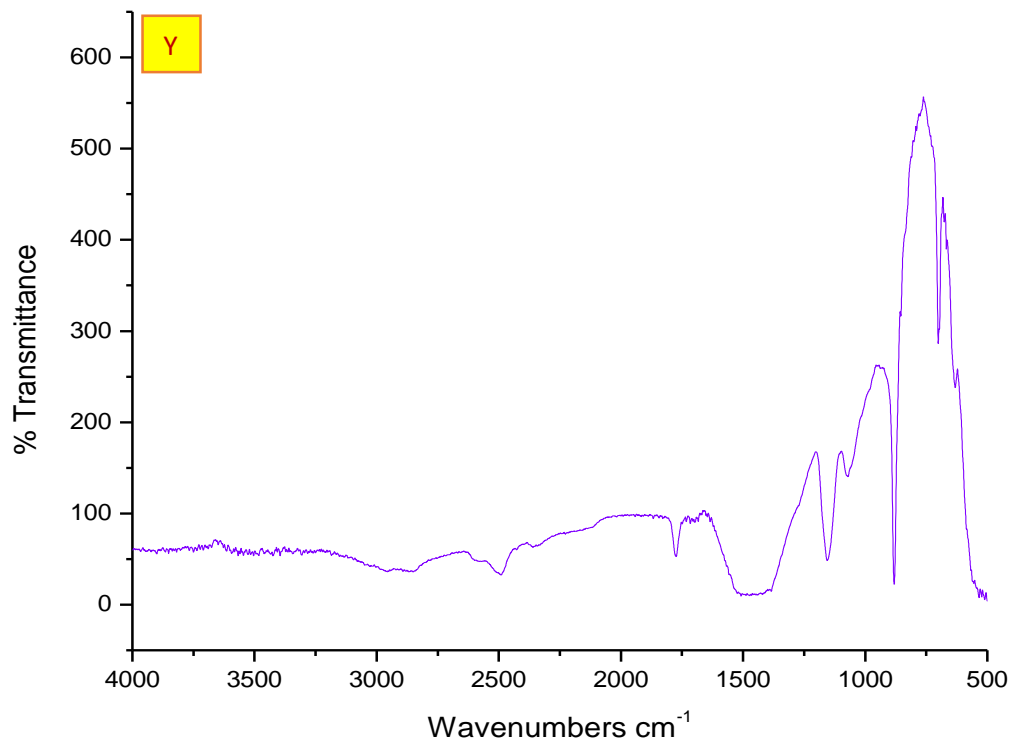
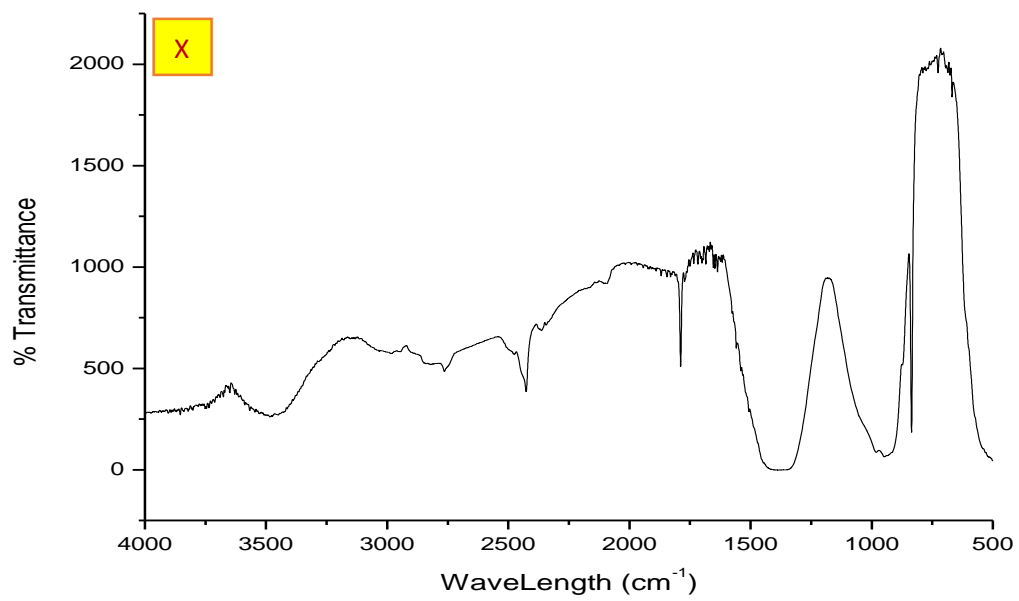


Figure 4.1: FTIR spectra for ZnO (X) and doped phyto-enhanced ZnO (Y)

4.3.2 Scanning electron microscopy (SEM)

Scanning electron microscope (SEM) has been reported to be one of the notable leading techniques for the determination of the topographical study of prepared samples. It provides vital facts about the morphological shape of synthesized samples. The SEM micrograph as shown in Figure 4.2, clearly displays the morphology of the nanoparticles produced. The SEM image for synthesized ZnO (X) revealed a network configuration of an agglomerated blend of elongated rod-like shapes and selfsame spheres. Whereas, the SEM micrograph of the doped phyto-enhanced ZnO nanoparticles (Y) revealed loosed structure of uniformly distributed particles with increased surface area as confirmed by the BET result. The nanoparticles were spherical, granular, sponge or flowerlike in nature. This is peculiar to ZnO nanoparticle obtained from *moringa oleifera* plant extract (Basnet *et al.*, 2018). The average particle size and average grain size of the doped phyto-enhanced zinc oxide nanoparticles were 279 nm and 188 nm respectively. In addition, the nanoparticles were inclined to aggregation or agglomeration due to the surface-to-volume ratio which is typical with phyto-enhanced nanoparticles as suggested in many literatures (Balogun *et al.*, 2020). This is because phyto-enhanced nanoparticles are known for their large surface area with notable inclination for attraction between particles (Barzinjy and Azeez, 2020). Remarkably, greater amount of the zinc oxide nanoparticles doped with graphitic carbon nitrite were identical in dimension.

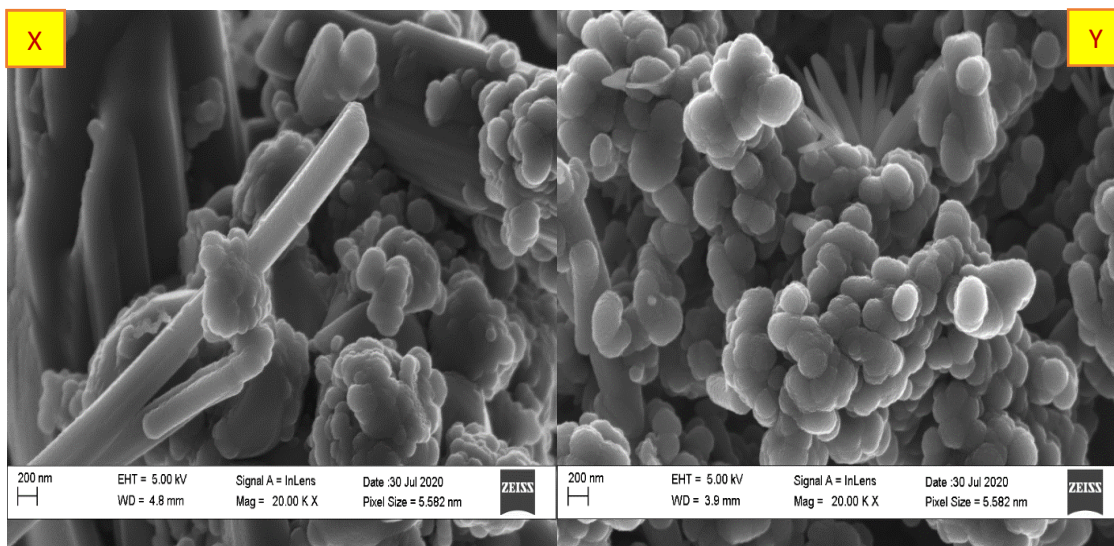


Figure 4.2: SEM micrograph of synthesized ZnO(X) and doped phyto-enhanced ZnO(Y)

4.3.3 Elemental composition (EDX) of the photocatalyst

The elemental composition of synthesized ZnO and that of doped phyto-enhanced ZnO nanoparticles with their respective atomic and weight percent were verified by energy dispersive X-ray (EDX) analysis. The observed spectra of the samples in figure 4.3, shows that it contains traces of impurities which is expected. The peak of zinc(Zn), oxygen(O), carbon(C), Sodium (Na), potassium(K) and Sulphur(S) were all observed for the synthesized ZnO. Whereas, it shows peaks of zinc(Zn), oxygen(O), carbon(C), sodium(Na), magnesium(Mg), phosphorous(P) and potassium(K) for the synthesized doped phyto-enhanced zinc oxide nanoparticle. The EDX spectra indicates three peaks for zinc(Zn) at 1, 8.6, and 9.6 keV respectively and a unique peak for oxygen at ~0.5 keV which is typical of ZnO NPs. Similar report was made by Barzinjy and Azeez, (2020). The observed peaks of Potassium(K), Sulphur(S), magnesium(Mg) and phosphorous(P) in traces could be due to surface contamination in the course of the analysis. The carbon peaks observed maybe attributed to the carbon composition of the storage material and the carbon introduced by the dopant. However, the observed spectrum of sodium is a misidentification of Zn as Na. Similar observation was made by Newbury (2009). The absence of nitrogen in the synthesized doped phyto-enhanced zinc oxide nanoparticle

could be attributed to the deamination during thermal polymerization reaction (Paul *et al.*, 2020). Theoretically as reported by Bari *et al.*, (2009), the anticipated weight percent of Zn and O for raw zinc oxide (ZnO) synthesized nanoparticles are 80.3% and 19.7% respectively. Although in this work the weight percentage of these two elements was not close to the expected values because of these contaminations aforementioned earlier. However, it did not in any way affect the photocatalytic performance of the synthesized doped zinc oxide nanoparticles as shown in Figure 4.3.

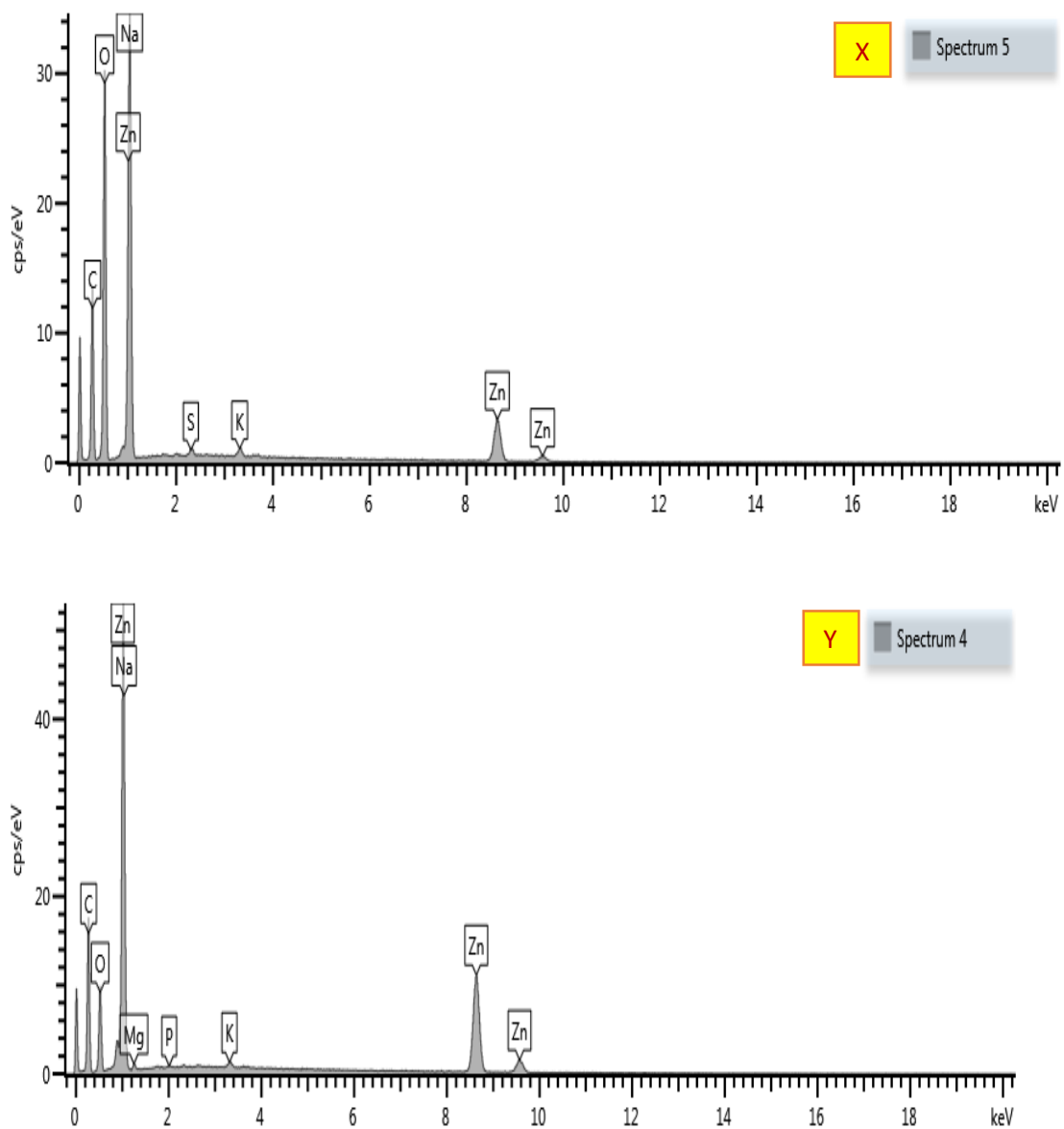


Figure 4.3: EDX spectrum of synthesized ZnO (X) and doped phyto-enhanced ZnO (Y)

4.3.4 XRD pattern of the photocatalyst

Figure 4.4 presents the mineralogical composition and crystallinity of the photocatalysts. The XRD pattern clearly indicates crystalline structure for synthesized ZnO and doped phyto-enhanced ZnO nanoparticles. The 2θ values corresponding to the observed diffraction peaks were 31.78, 34.46, 36.28, 47.54, 56.60, 62.92 and 68.00 degrees for synthesized ZnO (X) whereas 2θ values 31.71, 34.49, 36.28, 47.64, 56.60, 62.99 and 68.13 degrees for doped phyto-enhanced ZnO nanoparticles (Y).

These peaks correspond to the miller index (100), (002), (101), (102), (110), (103) and (112) in that order. This confirms the structure (hexagonal wurtzite) of the synthesized ZnO and doped phyto-enhanced ZnO NPs (Fakhari *et al.*, 2019). The XRD configuration of synthesized ZnO was in cognate with the doped phyto-enhanced ZnO which suggests that doping did not alter the crystal structure of ZnO (Zhang *et al.*, 2019).

The doping of g-C₃N₄ into the ZnO lattice generated residual stress in the matrix which led to the slight shift in characteristic peaks observed in the 2θ values of doped nanoparticles (Ansari *et al.*, 2017). This typical diffraction patterns of synthesized ZnO and doped ZnO nanoparticles according to Guan *et al.*, (2019) are well consistent and shows strong alignment with the JCPDS standard card for ZnO (JCPDS: 36-1451). Although the XRD pattern of the doped phyto-enhanced ZnO showed that the characteristic peaks depicting ZnO can be visibly seen, but no notable peaks of the dopant were detected.

This absence of the dopant can be as a result of relatively low proportion of the dopant in the doping ratio. This is in agreement to the report of Li *et al.*, (2019); and Cao *et al.*, (2017). The introduction of the dopant did not affect the crystallinity and structure of ZnO (Gionco *et al.*, 2016). The crystalline sizes of synthesized zinc oxide and the doped phyto-

enhanced ZnO nanoparticles in Figure 4.4 were calculated as 29.87 nm and 30.27 nm using Deybe-Scherer's Equation. This is a confirmation of the slight shift observed. This is in agreement with the report of El-Bindary *et al.*; (2019).

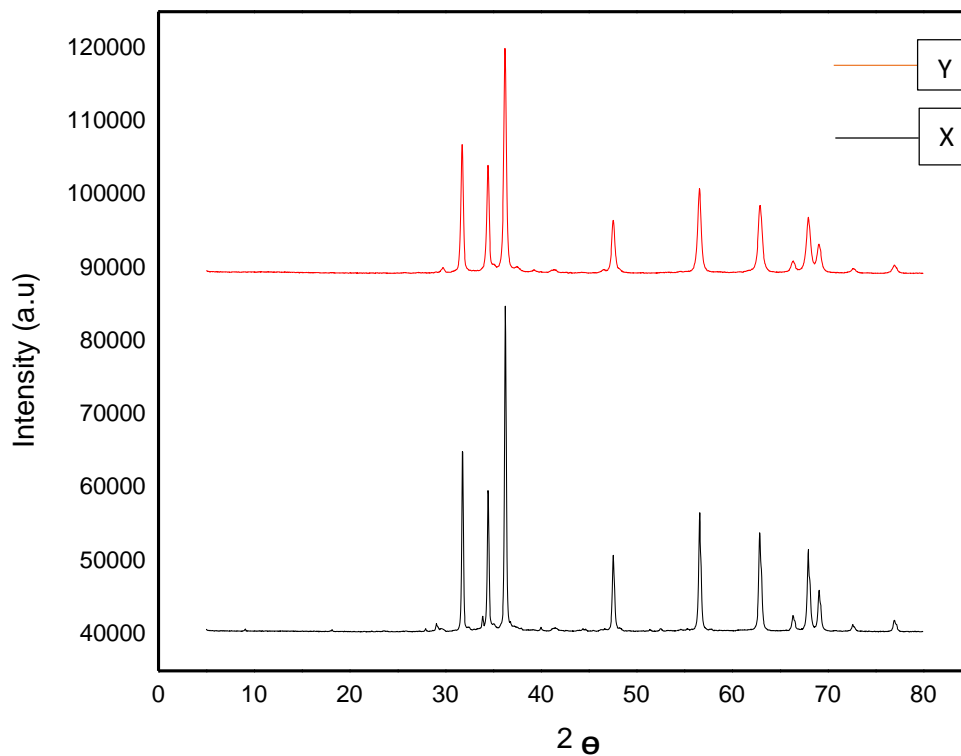


Figure 4.4: XRD spectrum of synthesized ZnO (X) and doped phyto-enhanced ZnO (Y)

4.3.5 Surface area identification using BET

The surface area, pore volume and diameter of the photocatalyst are represented in Table 4.3. DR's method micropore area of Brunauer-Emmett-Teller (BET) plots calculated surface area of synthesized zinc oxide and doped phyto-enhanced zinc oxide as 35.44 m²/g and 346.1 m²/g respectively. The doped phyto-enhanced zinc oxide nanoparticle was characterized by high surface area which was approximately 10 times greater than the pure sample. The increased surface area is a clear outcome of morphological evolution caused by phyto-enhancement which could have led to reduction in grain size, leading to

an increased surface area. Similar report was made by Li *et al.*, (2019). Larger surface area offered adsorption of more organic pollutants on the surface of the photocatalyst, thus improving photocatalytic activity. Barzinjy *et al.*, (2020) made similar report. Furthermore, the pore diameter and pore volume for the synthesized zinc oxide and the doped phyto-enhanced zinc oxide was also estimated with the help of the Barret-Joyner-Halenda method. For the synthesized zinc oxide, the pore diameter and pore volume was 2.965 nm and 0.01259 cm³/g respectively whereas the pore diameter and pore volume for the doped phyto-enhanced zinc oxide was 5.428 nm and 0.123 cm³/g respectively as seen on Table 4.4. This improvement is an attestation to the remarkable degradation that was observed in this work.

Table 4.4: BET Summary

Photocatalyst	Surface area (m ² /g)	Pore diameter (nm)	Pore volume (cm ³ /g)
Synthesized ZnO	35.44	2.965	0.01259
Doped phyto-enhanced ZnO	346.1	5.428	0.123

4.4 Effect of Operating Parameters on Photocatalysis

4.4.1 Effect of photocatalyst loading on the degradation of tetracycline solution

It has been vastly reported that rate and efficiency of degradation is affected by photocatalyst loading. Different photocatalyst dosage range of 0.1 - 0.5 g/L were employed in a batch experiment to analyze this effect on tetracycline degradation. It is observed that with increase in the photocatalyst loading, there is a corresponding increase in tetracycline degradation. This phenomenon may be attributed to effective catalyst surface area made available for light absorption resulting in increased active site of the photocatalyst. As shown in Figure 4.5, 0.2 g/L was the best dosage with the highest rate of removal. Thereafter, a sharp reduction in the removal efficiency was observed. At 0.2 g/L dosage, the quantity of visible light irradiation absorbed from the sun and the high

proportion of tetracycline molecules adsorbed to the many available active site of the catalyst surface is responsible for the 98% removal efficiency. Therefore, adequate photocatalyst loading can increase the inducement of electron/hole pairs, consequent to improved photodegradation (Wang *et al.*, 2018). Also, as the dosage moved beyond the optimum, aggregation of photocatalyst was observed leading to a reduction in light penetration and the number of available active sites. Furthermore, this overloading led to increased solution turbidity which hindered the penetration of light due to scattering effect consequently resulting in shrinkage of the effective photoactivated volume of suspension. Owing to these reasons, the photocatalytic degradation beyond the optimum witnessed a reduction rather than linearly increasing (Lam *et al.*, 2012).

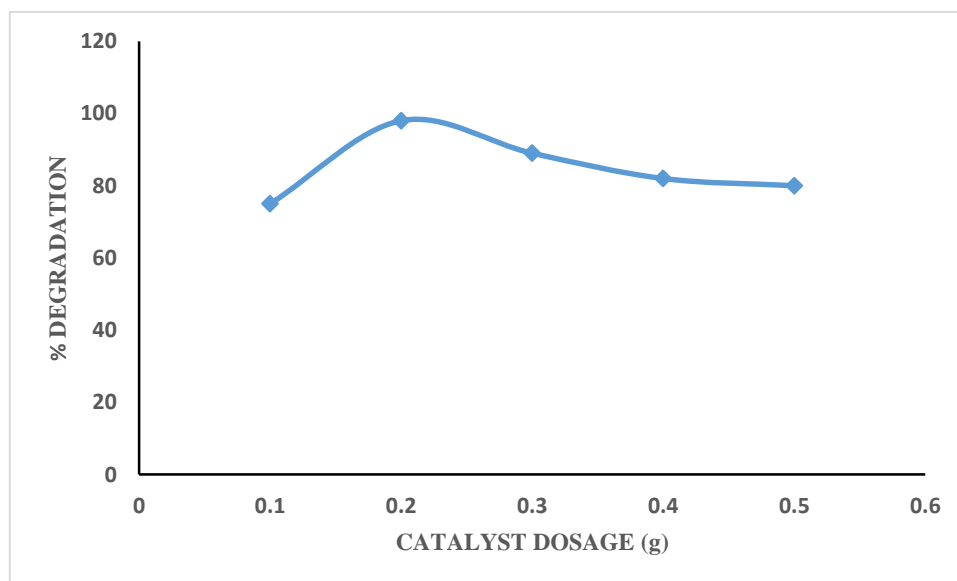


Figure 4.5: Effect of catalyst loading on degradation

4.4.2 Effect of solution pH

The solution pH is an essential parameter in photocatalysis. It dictates the mode of adsorption of the targeted molecules and its subsequent photocatalytic degradation by influencing the ionization state vis-a-viz the electrical charge characteristics of the photocatalyst surface. Figure 4.6 shows the removal rates of tetracycline by the

photocatalyst at varied solution pH of 2.0, 4.0, 6.0, 8.0, 10.0 and 12.0 respectively. The respective solution pH was adjusted using NaOH and HCl. At lower pH, degradation of tetracycline was low while, at higher pH, the degradation was relatively high. This may be due to the behavior of tetracycline at different pH and the surface-charge properties of the photocatalyst explained by point zero charge. At $\text{pH} < 3.3$, tetracycline exists in a cationic form; at $\text{pH} = 3.3 \sim 7.7$, as zwitterion; at $\text{pH} > 7.7$, as anion. Consequently, as pH increases, the proportion of the negative charge in the TC molecule increases (Chang *et al.*, 2015). However, the pH of zero-point charge (pHzpc) of the photocatalyst is estimated at 9.3. Accordingly, the photocatalyst surface is protonated below pH 9 and above this pH, catalyst surface is predominantly negatively charged by adsorbed OH^- ions (Lam *et al.*, 2012).

Hence it is logical that the optimum pH observed was 8 since at this pH slightly below the point zero charge, the surface of the photocatalyst is highly positive charged and conducive for photoelectron transfer even as the tetracycline molecule is highly anionic. At the optimum pH, electrostatic attraction between the positively charged surface of the photocatalyst and tetracycline anion was responsible for the high degradation obtained. In contrast, as pH increased more than 8, the photocatalyst surface becomes negatively charged resulting in electrostatic repulsion with the anionic targeted molecules. This is responsible for the reduced photodegradation (Chen *et al.*, 2017; Saadati *et al.*, 2016).

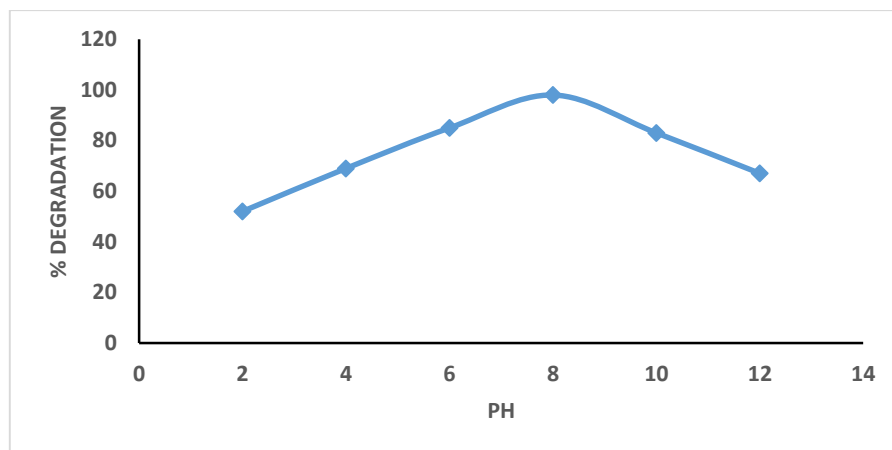


Figure 4.6: Effect of pH on degradation percentage

4.4.3 Effect of initial concentration

The effect of varying tetracycline concentration (5 – 20 mg/L) on photocatalytic degradation efficiency of tetracycline was investigated at initial pH value of 8, irradiation time of 180 min and doped phyto-enhanced zinc oxide photocatalyst dosage of 0.2 g/L. Figure 4.7 shows the influence of initial TC concentration on the removal efficiency of tetracycline. The results showed that the removal efficiency decreased with the increasing initial TC concentration. Irradiation of TC solution with the initial concentrations of 5, 10, 15 and 20 ppm for 180 min led to degradation of 98.7, 98.0, 92.0 and 90.0% of TC, reflecting lower removal efficiency at higher TC concentrations. Moreover, with increasing initial TC concentration, more TC molecules were adsorbed on the surface of doped phyto-enhanced zinc oxide nanoparticles. The high amount of adsorbed TC led to an inhibitive influence on the reaction of TC molecules with photogenerated holes or hydroxyl radicals, due to the lack of direct contact between them. This could be due to the increase in internal optical density, which resulted in the solution becoming impervious to sunlight (Sin *et al.*, 2011). Furthermore, increasing TC concentration led to the absorption of light by the TC molecules, and thereby, the photons never reached the photocatalyst surface, and the photocatalytic removal efficiency decreased. This is in

line with the report of Mohammadi *et al.*, (2012). In addition, the reduction in removal efficiency with increasing initial TC concentration could be due to the fact that under the same conditions, the amount of reactive radicals formed was equal in all solutions; therefore, the reaction of TC molecules with radicals becomes more likely at lower TC concentrations. This can lead to a decrease in the degradation efficiency of TC molecules (Nosrati *et al.*, 2012). This result is similar with results obtained by Gomez-Pacheco *et al.*, (2012) and Jiao *et al.*, (2008b), who studied the degradation of TC using UV irradiation and concluded that the TC photolysis rate constants decreased with increase of the initial concentration of TC. In another study, Klauson *et al.*, (2010), who studied amoxicillin (AMX) degradation in the range 10–100 mg/L with 1 g/L Degussa P25 under UV-A, reported that with increasing AMX concentration, degradation rate decreased from 90 to 30% at 10 and 100 mg/L, respectively.

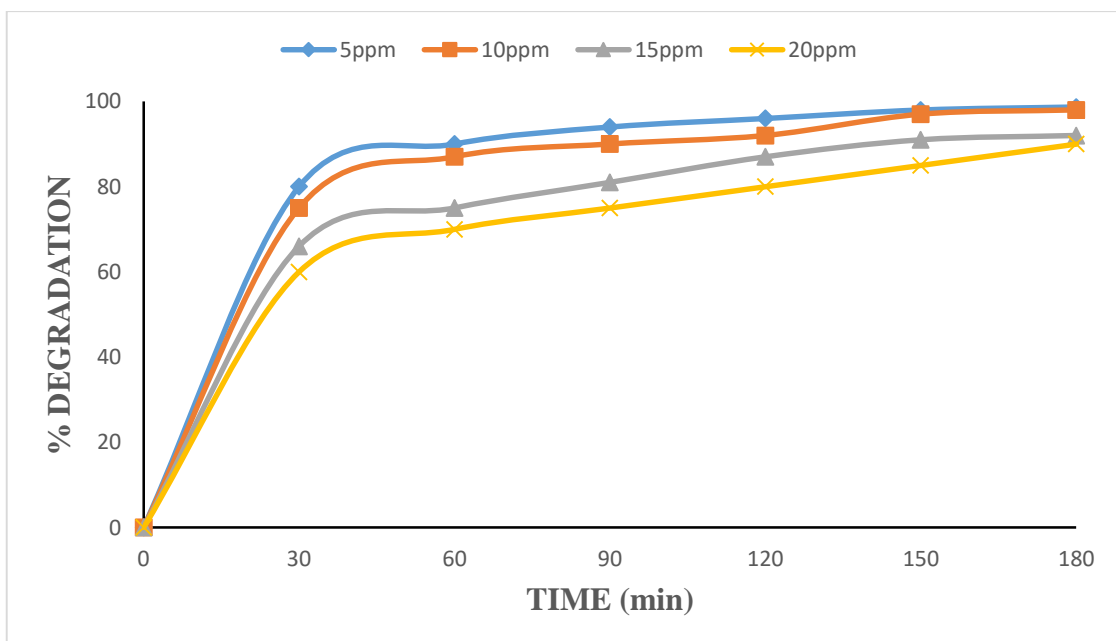


Figure 4.7: Effect of initial concentration on percentage degradation of tetracycline

4.5 Kinetic Study

In order to quantitatively investigate the degradation rate of TC over phyto-enhanced doped zinc oxide photocatalyst nanoparticle, the experimental data fitted by pseudo-first-

order kinetics and the fitting results showed (Table 4.5) that TC degradation rate constants (k) were calculated to be 0.0221, 0.0196, 0.013 and 0.011 min⁻¹ at initial TC concentration of 5, 10, 15, and 20 ppm, respectively. This was evaluated over 180 min time interval 0.2 g/L, and pH 8.

The increase in initial TC concentration led to the decrease of the TC degradation rate constants. This could be due to the transition from the kinetic control regime at low concentrations to mass transfer limitations at high concentrations. Also at higher concentrations, because of increasing concentrations of intermediate products, hydroxyl radicals became the limiting reactant and so degradation rate constants decreased (Dimitrakopoulou *et al.*, 2012). Figure 4.8 shows a plot of $\ln(C_o/C_t)$ versus time (t). The plot is fitted with a straight line using linear regression techniques. The linear fit observed was a confirmation of pseudo first order kinetic behavior with the $R^2 > 0.92$ which indicates that the photodegradation of tetracycline fits well with the kinetic model. The closeness of the correlation constant to unity indicates that the degradation process follows pseudo first order kinetics and this is well represented by the Langmuir—Hinshelwood model (Chen *et al.*, 2017a).

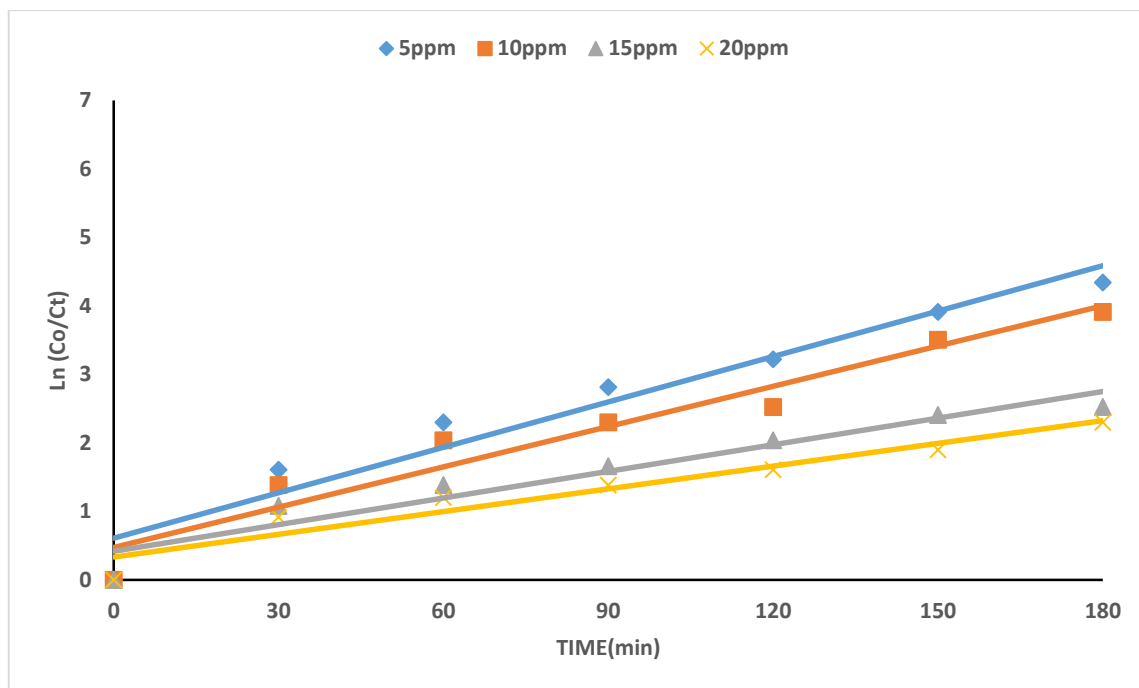


Figure 4.8: Kinetics of tetracycline degradation under sunlight in the presence of doped phyto-enhanced zinc oxide nanoparticles.

Table 4.5: Kinetic Parameters for Photocatalytic Degradation of Tetracycline

Concentration (ppm)	Equation	Rate constant (k)	R ²
5	$y = 0.0221x + 0.6124$	0.0221	0.9441
10	$y = 0.0196x + 0.4753$	0.0196	0.9423
15	$y = 0.013x + 0.419$	0.013	0.924
20	$y = 0.011x + 0.3371$	0.011	0.9297

4.6 Proposed Reaction Mechanism

Reactions can be initiated with the absorption of light by a doped phyto-enhanced zinc oxide (ZnO) photocatalyst from any light source (sunlight or illuminated light source) (Sacco *et al.*, 2018). This exposure leads to the production of electrons and holes pairs by photons with energy greater or equal to the band energy of the photocatalyst. The electrons which are excited by the light spectrum (photons), migrate from the valence

band (VB) to the conduction band (CB) due to excess energy acquired, thereby creating pairs of photoelectrons (e^-) and photo-holes (h^+) (Akpan and Hameed, 2009).

The holes must be positive enough to generate reactive species radicals (RSr) like hydroxyl radicals (OH^\cdot) and the electrons must be negative enough to reduce the oxygen molecules present in the aqueous solution which subsequently generates series of OH^\cdot (Ng and Cheng, 2017). The radicals are adsorbed/generated at the active sites of the photocatalyst; thus, the pollutants that are also adhered to the active sites are mineralized by successive radical reactions to nontoxic substances.

The only challenge that can be encountered during the process is the recombination of the electrons and holes which is accompanied with emission of heat, within nanoseconds (Dong *et al.*, 2015) and hinders the generation of the key driving force of the process (RSr), which are common with facile semiconductors mostly with large or small band gap. Also, this can occur if the oxygen concentration is low, therefore electrons are not caught (absence of electron acceptors and donors) (Yasmina *et al.*, 2014). Prevention of recombination of e^- and h^+ allows the formation of superoxide ($O_2^{\cdot-}$) and other RSr which speeds up the photocatalytic redox reactions (Akpan and Hameed, 2009; García-Fernandez *et al.*, 2015; Yasmina *et al.*, 2014). Eqs. (1) to (10) summarizes the reaction mechanism in photocatalysis (Akpan and Hameed, 2009; Chong *et al.*, 2010).

1. Absorption of efficient photons ($h\nu \geq E_G = 3.2 \text{ eV}$) by Zinc Oxide



2. Oxygen ionosorption (first step of oxygen reduction)



3. Neutralization of OH^- groups by photoholes which produces OH^\cdot radicals



4. Neutralization of $O_2^{\circ-}$ by protons



5. Transient hydrogen peroxide formation and dismutation of oxygen



6. Decomposition of H_2O_2 and second reduction of oxygen



7. Oxidation of the organic reactant via successive attacks by OH° radicals



8. Direct oxidation by reaction with holes



9. As an example of the last process, holes can react directly with carboxylic acids generating CO_2



10. Expected overall reaction



Based on the above, the rate limiting steps in this mechanism are equations 4.1, 4.2, 4.3, 4.6, 4.7 and 4.8.

CHAPTER FIVE

5.0 CONCLUSION AND RECOMMENDATIONS

5.1 Conclusion

In this study, the following conclusions were made:

Zinc oxide was successfully prepared using precipitation method. Subsequently, phyto-enhancement and doping of the prepared zinc oxide with graphitic carbon nitride was successfully done via physical mixing method.

The pure zinc oxide and doped phyto-enhanced photocatalyst produced were characterized by SEM-EDX, FTIR, BET, and XRD. The morphology of the photocatalyst at different magnifications confirmed that ZnO nanoparticles were formed. However, the doped phyto-enhanced zinc oxide micrograph revealed loosed structure of uniformly distributed particles with increased surface area. Although the EDX confirmed the elemental presence of Zn and O, it also revealed some impurities which were as a result of surface contamination and storage material of sample before analysis. The FTIR spectrum suggests the existence of functional groups typical of zinc oxide nanoparticle with registered peaks of graphitic carbon nitride in the doped phyto-enhanced zinc oxide. The XRD pattern of ZnONPs shows the peaks indexed to ZnO with the hexagonal wurtzite structure and the average grain size of the particles was estimated to be 30.27 nm using Debye Scherer's equation. Additionally, the XRD analysis has revealed a peak shift to higher 2θ values, which is indicative of substitutional carbon nitride doping. The BET analysis revealed the surface area of doped phyto-enhanced zinc oxide to be 10 times greater than the pure zinc oxide confirming that phyto-enhancement and doping resulted in an enhanced surface area, leading to increased active sites. This result is a good indicator that the photocatalyst possesses considerable active adsorption sites to absorb tetracycline.

The produced photocatalyst was successfully used to degrade tetracycline in a simulated solution o tetracycline. The results of this degradation shows that tetracycline removal largely depends on operating parameters as 98% degradation was recorded with the catalyst dosage of 0.2 g/L and pH 8 as optimum conditions.

Based on the results obtained from this work, it can be concluded that phyto-enhancement and doping with suitable non-metal ion like graphitic carbon nitride have reduced the energy gap, enhanced photo-generated electron–hole pairs, reduced frequency of photo-induced charge recombination which in turn led to a better photoactivity of the zinc oxide nanoparticle under sunlight for photocatalytic degradation of tetracycline.

The kinetic study showed the closeness of the correlation constant to unity which indicates that the degradation process follows pseudo first order kinetics and is well represented by the Langmuir—Hinshelwood model.

It has been proven by this technique that irradiation from the sun can achieve the same work as UV Lamps. Hence as compared with UV lamps, the use of sunlight on large scale is more economical and has less strategic problems.

5.2 Recommendations

Despite extensive investigations, it is suggested that:

- I. Future studies should focus on immobilization of photocatalyst on suitable support matrices (powder/pellet substrates, soft/thin materials, or on rigid/thick substrates) to prevent the post separation and recovery of the catalyst particles from the reaction mixture in aqueous slurry systems.
- II. Furthermore, a reasonable designed photocatalytic reactor can reduce energy consumption or can prevent post separation stages in photocatalytic processes.
- III. Additionally, most of the photocatalytic studies concentrate only on the degradation rate and efficiency of target organic pollutants disregarding the toxicity issues of the degradation intermediates. Introducing the High-Performance Liquid Chromatography (HPLC) to detect the intermediates in the photocatalytic process should be considered

- IV. A demonstrated ability to use ZnO-based catalyst at a solar pilot scale for effluent purification processes would certainly benefit the commercial sector both in terms of environment and economy.
- V. Operating parameters such as the effects of mass mixing ratio/optimum volume of the leaf extract in the solution and the calcination temperature on the morphology of the modified ZnO nanoparticles should be examined
- VI. The band gap energy of the doped phyto-enhanced ZnO photocatalyst as well as the effect of different plant extract on the band gap energy should be examined

5.3 Contribution to Knowledge

In this research a new doping method which involved physically mixing green synthesized ZnO with graphitic carbon nitrite (g-C₃N₄) at a doping ratio of 5% w/w was developed. The developed method reduced the bandgap of ZnO from 3.37 eV to 3.20 eV which is within the visible light region. The effect of green synthesis and doping led to 98% degradation of tetracycline after 3 hours. The success of this research also demonstrated the potency of sunlight as a viable alternative to conventional UV light.

REFERENCES

- Abdollahi, Y., Abdullah, A. H., U. I. Gaya, Z., Zainal & Yusof N. A. (2012). Enhanced photodegradation of o-cresol in aqueous Mn (1%)-doped ZnO suspensions, *Environmental Technology*, 33:10, 1183-1189
- Adhikari, R., Gyawali, G., Cho, S. H., Narro-García, R., Sekino, T., & Lee, S. W. (2014). Er³⁺/Yb³⁺ co-doped bismuth molybdate nanosheets upconversion photocatalyst with enhanced photocatalytic activity. *Journal of Solid State Chemistry*, 209, 74-81.
- Akpan, U. G, & Hameed, B. H. (2009). Parameters affecting the photocatalytic degradation of dyes using TiO₂-based photocatalysts: A review, *Journal of Hazardous Materials* 170 (2009) 520–529

- Akpan, U. G, & Hameed, B. H. (2011). Enhancement of the photocatalytic activity of TiO₂ by doping it with calcium ions. *Journal of Colloid and Interface Science* 357, 168–178
- Ahmadi, M., Motlagh, H. R., Jaafarzadeh, N., Mostoufi, A., Saeedi, R., Barzegar, G., & Jorfi, S. (2017). Enhanced photocatalytic degradation of tetracycline and real pharmaceutical wastewater using MWCNT/TiO₂ nano-composite. *Journal of environmental management*, 186, 55-63.
- Ahmadi, M., Ghanbari, F., & Madihi-Bidgoli, S. (2016). Photoperoxi-coagulation using activated carbon fiber cathode as an efficient method for benzotriazole removal from aqueous solutions: modeling, optimization and mechanism. *Journal of Photochemistry and Photobiology A: Chemistry*, 322, 85-94.
- Ahmadi, M., Amiri, H., & Martínez, S. S. (2012). Treatment of phenol-formaldehyde resin manufacturing wastewater by the electrocoagulation process. *Desalination and Water Treatment*, 39(1-3), 176-181.
- Ahmed, S., et al., (2015). Green synthesis of silver nanoparticles using *azadirachta indica* aqueous leaf extract, *Journal of Radiation Research and Applied Sciences*, <http://dx.doi.org/10.1016/j.jrras.2015.06.006>
- Ajala, F., Hamrouni, A., Houas, A., H. Lachheb, B. Megna, L. Palmisano, & F. Parrino. (2018). The influence of Al doping on the photocatalytic activity of nanostructured ZnO: *The role of adsorbed water*, *Applied Surface Science* (2018), doi: <https://doi.org/10.1016/j.apsusc.2018.03.141>
- Ameta, R., Chohadia, A. K., Jain, A., & Punjabi, P. B. (2018). Fenton and photo-fenton processes. In *Advanced oxidation processes for waste water treatment* (pp. 49-87).
- Ani, I. J., Akpan, U. G., Olutoye, M. A., & Hameed, B. H. (2018). Photocatalytic degradation of pollutants in petroleum refinery wastewater by TiO₂-and ZnO-based photocatalysts: Recent development. *Journal of cleaner production*, 205, 930-954.
- Anirudhan, T. S., & Deepa, J. R. (2017). Nano-zinc oxide incorporated graphene oxide/nanocellulose composite for the adsorption and photo catalytic degradation of ciprofloxacin hydrochloride from aqueous solutions. *Journal of colloid and interface science*, 490, 343-356.
- Anju, S. G. (2012). Sono, photo and sonophoto Catalytic Removal of chemical and bacterial pollutants from wastewater, *Thesis submitted to Cochin University of Science and Technology*. Kochi - 682 022
- Ansari, S. A., Ansari, S. G., Foad, H., & Cho, M. H. (2017). Facile and sustainable synthesis of carbon-doped ZnO nanostructures towards the superior visible light photocatalytic performance. *New Journal of Chemistry*, 41(17), 9314-9320.
- Aydin, S., Ince, B., & Ince, O. (2015). Development of antibiotic resistance genes in microbial communities during long-term operation of anaerobic reactors in the treatment of pharmaceutical wastewater. *Water Research*, 83, 337-344.

- Balogun, S. W., James, O. O., Sanusi, Y. K., & Olayinka, O. H. (2020). Green synthesis and characterization of zinc oxide nanoparticles using bashful (*Mimosa pudica*), leaf extract: a precursor for organic electronics applications. *Sn Applied Sciences*, 2(3), 1-8.
- Bari, A. R., Shinde, M. D., Vinita, D. & Patil, L. A. (2009). Effect of solvents on the particle morphology of nanostructured ZnO. *Indian Journal of Pure & Applied Physics*, 47, 24-27.
- Baruah, S., & Dutta, J. (2009). Hydrothermal growth of ZnO nanostructures. *Science and technology of advanced materials*.
- Barzinjy, A. A., & Azeez, H. H. (2020). Green synthesis and characterization of zinc oxide nanoparticles using *Eucalyptus Globulus labill* leaf extract and zinc nitrate hexahydrate salt. *SN Applied Sciences*, 2(5), 1-14.
- Basnet, P., Chanu, T. I., Samanta, D., & Chatterjee, S. (2018). A review on bio-synthesized zinc oxide nanoparticles using plant extracts as reductants and stabilizing agents. *Journal of Photochemistry and Photobiology B: Biology*, 183, 201-221.
- Biasotto, G., Ranieri, M.G.A., Foschini, C. R., Simes A. Z., Longo, E., & Zaghete M. A. (2014) Gas sensor applications of zinc oxide thin film grown by the polymeric precursor method, 14991–14996. doi: 10.1016/j.ceramint.2014.06.099
- Byzynski, G., Andreza, P. P., Diogo, P. V., Caue, R., Elson L. (2017). High-performance ultraviolet-visible driven ZnO morphologies photocatalyst obtained by microwave-assisted hydrothermal method, *Journal of Photochemistry and Photobiology A: Chemistry* <https://doi.org/10.1016/j.jphotochem.2017.11.032>
- Cao, Z., Zhang, J., Zhou, J., Ruan, X., Chen, D., Liu, J., & Qian, G. (2017). Electroplating sludge derived zinc-ferrite catalyst for the efficient photo-fenton degradation of dye. *Journal of environmental management*, 193, 146-153.
- Chang, C. C., Yang, M. H., Wen, H. M., & Chern, J. C. (2002). Estimation of total flavonoid content in propolis by two complementary colorimetric methods. *Journal of food and drug analysis*, 10(3).
- Chang, P. H., Jiang, W. T., Li, Z., Jean, J. S., & Kuo, C. Y. (2015). Antibiotic tetracycline in the environments—A review. *Research & Reviews: Journal of Pharmaceutical Analysis*, 4(3), 86-111.
- Chen, C., Li, Y., Ma, W., Guo, S., Wang, Q., & Li, Q. X. (2017). Mn-Fe-Mg-Ce loaded Al₂O₃ catalyzed ozonation for mineralization of refractory organic chemicals in petroleum refinery wastewater. *Separation and Purification Technology*, 183, 1-10.
- Chen, X., Wu, Z., Liu, D., & Gao, Z. (2017a). Preparation of ZnO photocatalyst for the efficient and rapid photocatalytic degradation of azo dyes. *Nanoscale research letters*, 12(1), 1-10.
- Chemingui, H., Missaoui, T., Mzali, J. C., Yildiz, T., Konyar, M., Smiri, M., & Yatmaz, H. C. (2019). Facile green synthesis of zinc oxide nanoparticles (ZnO NPs):

Antibacterial and photocatalytic activities. *Materials Research Express*, 6(10), 1050b4.

- Cho, S., Jang, J. W., Lee, J. S., & Lee, K. H. (2010). Carbon-doped ZnO nanostructures synthesized using vitamin C for visible light photocatalysis. *CrystEngComm*, 12(11), 3929-3935.
- Chong, M.N., Jin, B., Chow, C. W., & Saint, C. (2010). Recent developments in photocatalytic water treatment technology: A review. *Journal of Water Research*, 44 (10), 2997–3027.
- Cicco, N., Lanorte, M. T., Paraggio, M., Viggiano, M., & Lattanzio, V. (2009). A reproducible, rapid and inexpensive Folin–Ciocalteu micro-method in determining phenolics of plant methanol extracts. *Microchemical journal*, 91(1), 107-110.
- Dimitrakopoulou, D., Rethemiotaki, I., Frontistis, Z, Xekoukoulotakis, NP, Venieri, D, & Mantzavinos, D. (2012). Degradation, mineralization and antibiotic inactivation of amoxicillin by UV-A/TiO₂ photocatalysis. *J Environ Manag* 98(1):168–174
- Diya'uddeen, B. H., Wan Mohd, W., Wan, A., Daud, A.R., & Aziz A. (2011). Treatment technologies for petroleum refinery effluents: A review, *Process Safety and Environmental Protection* 89 (2011) 95–105
- Dong, H., Zeng, G., Tang, L., Fan, C., Zhang, C., He, X., & He, Y. (2015). An overview on limitations of TiO₂-based particles for photocatalytic degradation of organic pollutants and the corresponding countermeasures. *Water research*, 79, 128-146.
- El-Bindary, A. A., Ismail, A., & Eladl, E. F. (2019). Photocatalytic degradation of reactive blue 21 using Ag doped ZnO nanoparticles.
- Fakhari, S., Jamzad, M., & Kabiri Fard, H. (2019). Green synthesis of zinc oxide nanoparticles: a comparison. *Green chemistry letters and reviews*, 12(1), 19-24.
- García-Fernández, I., Fernández-Calderero, I., Polo-López, M. I., & Fernandez-Ibanez, P. (2015). Disinfection of urban effluents using solar TiO₂ photocatalysis: a study of significance of dissolved oxygen, temperature, type of microorganism and water matrix. *Catalysis today*, 240, 30-38.
- Gionco, C., Fabbri, D., Calza, P., & Paganini, M. C. (2016). Synthesis, characterization, and photocatalytic tests of N-doped zinc oxide: A new interesting photocatalyst. *Journal of Nanomaterials*, 2016.
- Gomez-Pacheco C, Sanchez-Polo M, Rivera-Utrilla J, Lopez-Penalver J. (2012). Tetracycline degradation in aqueous phase by ultraviolet radiation. *Chem Eng J* 187(1):89–95
- Guan, R., Li, J., Zhang, J., Zhao, Z., Wang, D., Zhai, H., & Sun, D. (2019). Photocatalytic performance and mechanistic research of ZnO/g-C₃N₄ on degradation of methyl orange. *ACS omega*, 4(24), 20742-20747.
- Hameed, B. H, Akpan, U. G., & Wee, K. P. (2011): Photocatalytic degradation of Acid Red 1 dye using ZnO catalyst in the presence and absence of silver, *Desalination and Water Treatment*, 27: 204-209.

- He, H., & Zhou, Z. (2017). Electro-Fenton process for water and wastewater treatment. *Critical Reviews in Environmental Science and Technology*, 47(21), 2100-2131.
- Holkar, C. R., Jadhav, A. J., Pinjari, D. V., Mahamuni, N. M., & Pandit, A. B. (2016). J Environ Manage. A critical review on textile wastewater treatments: *Possible approaches*. 2016 Nov 1; 182:351-366. doi: 10.1016/j.jenvman.2016.07.090. Epub 2016 Aug 3. Review.
- Ibrahim, N.B, AL-Shomar, S. M., & Sahrim Ahmad, H. J. (2013): Effect of aging time on the optical, structural and photoluminescence properties of nanocrystalline ZnO films prepared by a sol-gel method, *Applied Surface Science* 283 (2013) 599-602
- Jiao S, Zheng S, Yin D, Wang L, & Chen L (2008b) Aqueous photolysis of tetracycline and toxicity of photolytic products to luminescent bacteria. *Chemosphere* 73(3):377-382
- Kalpana, V. N., & Devi Rajeswari, V. (2018). A review on green synthesis, biomedical applications, and toxicity studies of ZnO NPs. *Bioinorganic chemistry and applications*, 2018.
- Kaur, H., Kaur, S., Singh, J., Rawat, M., & Kumar, S. (2019). Expanding horizon: green synthesis of TiO₂ nanoparticles using *Carica papaya* leaves for photocatalysis application. *Materials Research Express*, 6(9), 095034.
- Keong, C. C., Vivek, Y. S., Salamatinia, B., & Horri, B. A. (2017, March). Green synthesis of ZnO nanoparticles by an alginate mediated ion-exchange process and a case study for photocatalysis of methylene blue dye. In *Journal of Physics: Conference Series* (Vol. 829, No. 1, p. 012014).
- Khan, W. Z., Imad, N., Madina, T., & Zhibeek, M. (2014): Refinery wastewater degradation with titanium dioxide, zinc oxide, and hydrogen peroxide in a photocatalytic reactor, *Process Safety and Environmental Protection* (2014) 121-149
- Khosravi, R., Ehrampoush, M. H., Moussavi, G., Ghaneian, M. T., Barikbin, B., Ebrahimi, A. A., & Sharifzadeh, G. (2019). Facile green synthesis of zinc oxide nanoparticles using *Thymus vulgaris* extract, characterization, and mechanism of chromium photocatalytic reduction. *Materials Research Express*, 6(11), 115093.
- Klauson D, Babkina J, Stepanova K, Krichevskaya M, & Preis S. (2010). Aqueous photocatalytic oxidation of amoxicillin. *Catal Today* 151(1):39-45
- Kong, J. Z., Zhai, H. F., Zhang, W., Wang, S. S., Zhao, X. R., Li, M., & Wu, D. (2017). Visible light-driven photocatalytic performance of N-doped ZnO/gC₃N₄ nanocomposites. *Nanoscale research letters*, 12(1), 1-10.
- Krishnan, S., Rawindran, H., Sinnathambi, C. M., & Lim, J. W. (2017). Comparison of various advanced oxidation processes used in remediation of industrial wastewater laden with recalcitrant pollutants. In *IOP Conference Series: Materials Science and Engineering* (Vol. 206, No. 1, p. 012089).

- Krishnakumar, B., Selvam, K., Velmurugan, R., & Swaminathan, M. (2010). Influence of operational parameters on photodegradation of Acid Black 1 with ZnO, *Desalin. Water Treat.* 24 (2010) 132–139.
- Kumar, A., Sharma, G., Naushad, M., Kumar, A., Kalia, S., Guo, C., & Mola, G. T. (2017). Facile hetero-assembly of superparamagnetic Fe₃O₄/BiVO₄ stacked on biochar for solar photo-degradation of methyl paraben and pesticide removal from soil. *Journal of Photochemistry and Photobiology A: Chemistry*, 337, 118-131.
- Lam, S. M., Sin, J. C., Abdullah, A. Z., & Mohamed, A. R. (2012). Degradation of wastewaters containing organic dyes photocatalysed by zinc oxide: a review. *Desalination and Water Treatment*, 41(1-3), 131-169.
- Lee, K. M., Lai, C. W., Ngai, K. S., & Juan, J. C. (2015). Recent development of zinc oxide based photocatalyst in water treatment technology: A Review, *Water Research* (2015), doi: 10.1016/j.watres.2015.09.045
- Li, K., Gao, S., Wang, Q., Xu, H., Wang, Z., Huang, B., & Lu, J. (2015). In-situ-reduced synthesis of Ti³⁺ self-doped TiO₂/g-C₃N₄ heterojunctions with high photocatalytic performance under LED light irradiation. *ACS applied materials & interfaces*, 7(17), 9023-9030.
- Li, T., Zhang, C. Z., Ding, D., Fan, X., & Li, Y. (2018). Experimental and theoretical study on degradation of oxidized C₆₀ in water via photo-fenton method. *Chemical Engineering Journal*, 334, 587-597.
- Li, X., Li, Y., Sun, G., Luo, N., Zhang, B., & Zhang, Z. (2019). Synthesis of a flower-like g-C₃N₄/ZnO hierarchical structure with improved CH₄ sensing properties. *Nanomaterials*, 9(5), 724.
- Li, Y., Yang, M., Xing, Y., Liu, X., Yang, Y., Wang, X., & Song, S. (2017). Preparation of carbon-rich g-C₃N₄ nanosheets with enhanced visible light utilization for efficient photocatalytic hydrogen production. *Small*, 13(33), 1701552.
- Liang, P., Zhang, C., Sun, H., Liu, S., Tadó, M., & Wang, S. (2016). Photocatalysis of C, N-doped ZnO derived from ZIF-8 for dye degradation and water oxidation. *RSC advances*, 6(98), 95903-95909.
- Liu, S., Li, C., Yu, J., & Xiang, Q. (2011). Improved visible-light photocatalytic activity of porous carbon self-doped ZnO nanosheet-assembled floers. *CrystEngComm*, 13(7), 2533-2541.
- Lupan, O., Guerin, V. M., Tiginyanu, I. M., Ursaki V. V., Chow L., & Heinrich H, Pauporte (2010). Well-aligned arrays of vertically oriented ZnO nanowires electrodeposited on ITO-coated glass and their integration in dye sensitized solar cells, *J. Photochem photobiol. A Chem.* 211 65-73.
- Matinise, N., Fuku, X. G., Kaviyarasu, K., Mayedwa, N., & Maaza, M. J. A. S. S. (2017). ZnO nanoparticles via *Moringa oleifera* green synthesis: Physical properties & mechanism of formation. *Applied Surface Science*, 406, 339-347.
- Manokari, M., & Shekhawat, M. S. (2016). Zinc oxide nanoparticles synthesis from *Moringa oleifera* Lam. Extracts and their characterization. *World Scientific News*, (55), 252-262.

- Manokari, M., & Shekhawat, M. S. (2017). Biosynthesis and characterization of zinc oxide nanoparticles using *Thunbergia erecta* (Benth.) T. Anders plant extracts. *Archives of Agriculture and Environmental Science*, 2(3), 148-51.
- Manokari, M., Latha, R., Priyadarshini, S., Cokul, R. M., Beniwal, P., & Shekhawat, M. S. (2019). Green synthesis of zinc oxide nanoparticles from aqueous extracts of *Sesamum indicum* L. and their characterization. *World News of Natural Sciences*, 23, 200-210.
- Meshram, S., Rohan, L., Shailesh, G., Shachi, N., Shirish, S., & Rajeev, C. (2011). Continuous flow photocatalytic reactor using ZnO–bentonite nanocomposite for degradation of phenol, *Chemical Engineering Journal* 172 (2011) 1008–1015. *Immobilization*
- Mhamdi, A, Labidi, A, Souissi, B., Kahlaoui, M., Yumak., Boubaker, K., Amlouk, A., & Amlouk, M. (2015). Impedance spectroscopy and sensors under ethanol vapors application of sprayed vanadium-doped ZnO compounds, *J. Alloys Compd.* 639 648–658. doi:10.1016/j.jallcom.2015.03.205
- Mohammadi R, Massoumi B, & Rabani M. (2012). Photocatalytic decomposition of amoxicillin trihydrate antibiotic in aqueous solutions under UV irradiation using Sn/TiO₂ nanoparticles. *Int J Photoenergy* 2012 1:1–11
- Newbury, D. E. (2009). Mistakes encountered during automatic peak identification of minor and trace constituents in electron-excited energy dispersive X-ray microanalysis. *Scanning: The Journal of Scanning Microscopies*, 31(3), 91-101.
- Ng, K. H., & Cheng, C. K. (2017). Photocatalytic degradation of palm oil mill effluent over ultraviolet-responsive titania: Successive assessments of significance factors and process optimization. *Journal of Cleaner Production*, 142, 2073-2083.
- Nikravan, A. (2015). Amoxicillin and ampicillin removal from wastewater by fenton and photo-fenton processes.
- Nosrati R, Olad A, & Maramifar R. (2012). Degradation of ampicillin antibiotic in aqueous solution by ZnO/polyaniline nanocomposite as photocatalyst under sunlight irradiation. *Environ Sci Pollut R* 19(6):2291–2299
- Ogunyemi, S. O., Abdallah, Y., Zhang, M., Fouad, H., Hong, X., Ibrahim, E., & Li, B. (2019). Green synthesis of zinc oxide nanoparticles using different plant extracts and their antibacterial activity against *Xanthomonas oryzae* pv. *oryzae*. *Artificial cells, nanomedicine, and biotechnology*, 47(1), 341-352.
- Patil, S. W. A. T. I., & Raut, S. J. (2012). Synthesis and characterization of ZnO nanoparticles and 50% ZnO-bentonite nanocomposite. *International Journal of Chemical Sciences*, 10(2), 1124-1132.
- Patil, S. S., Mali, M. G., Tamboli, M. S., Patil, D. R., Kulkarni, M. V., Yoon, H., & Kale, B. B. (2016). Green approach for hierarchical nanostructured Ag-ZnO and their photocatalytic performance under sunlight. *Catalysis Today*, 260, 126-134.
- Paul, D. R., Gautam, S., Panchal, P., Nehra, S. P., Choudhary, P., & Sharma, A. (2020). ZnO-modified g-C₃N₄: a potential photocatalyst for environmental application. *ACS omega*, 5(8), 3828-3838.

- Ping Liang, Chi Zhang, Hongqi Sun, Shaomin Liu, Moses Tade & Shaobin Wang, Photocatalysis of C, N-doped ZnO derived from ZIF-8 for dye degradation and water oxidation, *RSC Adv.*, 2016, 6, 95903-95909.
- Pirhashemi, M., & Habibi-Yangjeh, A. (2015): Ternary ZnO/AgBr/Ag₂CrO₄ nanocomposites with tandem n-n heterojunctions as novel visible-light-driven photocatalysts with excellent activity, *Ceramics International* 41 (2015) 14383–14393
- Priya, S. S., & Radha, K. V. (2017). A review on the adsorption studies off tetracycline onto various types of adsorbent. *Chemical Engineering Communication*, 204(8), 821-839.
- Rajendran, S. P., & Sengodan, K. (2017). Synthesis and characterization of zinc oxide and iron oxide nanoparticles using *Sesbania grandiflora* leaf extract as reducing agent. *Journal of Nanoscience*, 2017.
- Saadati, F., Keramati, N., & Ghazi, M. M. (2016). Influence of parameters on the photocatalytic degradation of tetracycline in wastewater: a review. *Critical reviews in environmental science and technology*, 46(8), 757-782.
- Sacco, O., Vaiano, V., Rizzo, L., & Sannino, D. (2018). Photocatalytic activity of a visible light active structured photocatalyst developed for municipal wastewater treatment. *Journal of Cleaner Production*, 175, 38-49.
- Sahu, H. N., & Sherikar, B. N. Synthesis of Fe Doped ZnO Spintronic Nano Powders by Solution Combustion Method & Their Characterization.
- Samadi, M., Zirak, M., Naseri, A., Khorashadizade, E., & Moshfegh, A. Z. (2016). Recent progress on doped ZnO nanostructures for visible-light photocatalysis. *Thin Solid Films*, 605, 2-19.
- Satyawali & Balakrishnan (2008). Wastewater treatment in molasses-based alcohol distilleries for COD and color removal: A review. *J Environ Manage.* 2008 Feb;86(3):481-97. Epub 2007 Feb 12
- Sawant, S. Y., & Cho, M. H. (2016). Facile and single-step route towards ZnO@ C core-shell nanoparticles as an oxygen vacancy induced visible light active photocatalyst using the thermal decomposition of Zn (an) 2 (NO 3) 2. *RSC advances*, 6(74), 70644-70652.
- Selvin, S. S. P., Radhika, N., Borang, O., Lydia, I. S., & Merlin, J. P. (2017). Visible light driven photodegradation of Rhodamine B using cysteine capped ZnO/GO nanocomposite as photocatalyst. *Journal of Materials Science: Materials in Electronics*, 28(9), 6722-6730.
- Sharmila, G., Thirumarimurugan, M., & Muthukumar, C. (2019). Green synthesis of ZnO nanoparticles using *Tecoma castanifolia* leaf extract: characterization and evaluation of its antioxidant, bactericidal and anticancer activities. *Microchemical Journal*, 145, 578-587.
- Shokry Hassan, H., Elkady, M. F., El-Shazly, A. H., & Bamufleh, H. S. (2014). Formulation of synthesized zinc oxide nanopowder into hybrid beads for dye separation. *Journal of nanomaterials*, 2014.

- Sin JC, Lam SM, Mohamed AR, Lee KT (2011) Degrading endocrine disrupting chemicals from wastewater by TiO₂. *Int J Photoenergy* 2012 1:1–23
- Sohrabi, M. R., Khavaran, A., Shariati, S., & Shariati, S. (2017). Removal of Carmoisine edible dye by fenton and photo fenton processes using taguchi orthogonal array design. *Arabian Journal of Chemistry*, 10, S3523-S3531
- Soltani, R. D. C., Khorramabadi, G. S., Khataee, A. R., & Jorfi, S. (2014). Silica nanopowders/alginate composite for adsorption of lead (II) ions in aqueous solutions. *Journal of the Taiwan Institute of Chemical Engineers*, 45(3), 973-980.
- Soltani, R. D. C., Jorfi, S., Ramezani, H., & Purfadakari, S. (2016). Ultrasonically induced ZnO–biosilica nanocomposite for degradation of a textile dye in aqueous phase. *Ultrasonics sonochemistry*, 28, 69-78.
- Soltani, R. D. C., Jorfi, S., Safari, M., & Rajaei, M. S. (2016). Enhanced sonocatalysis of textile wastewater using bentonite-supported ZnO nanoparticles: Response surface methodological approach. *Journal of environmental management*, 179, 47-57.
- Song, C., Chen, P., Wang, C., & Zhu, L. (2012). Photodegradation of perfluorooctanoic acid by synthesized TiO₂–MWCNT composites under 365 nm UV irradiation. *Chemosphere* 86, 853–859.
- Song, B., Zeng, Z., Zeng, G., Gong, J., Xiao, R., Ye, S., & Tang, X. (2019). Powerful combination of g-C₃N₄ and LDHs for enhanced photocatalytic performance: a review of strategy, synthesis, and applications. *Advances in colloid and interface science*, 272, 101999.
- Sun, J. H., Dong, S. Y., Feng, J. L., Yin, X. J., & Zhao, X. C. (2011). Enhanced sunlight photocatalytic performance of Sn-doped ZnO for Methylene Blue degradation. *Journal of Molecular Catalysis A: Chemical*, 335(1-2), 145-150.
- Thenarasu, G., & Sivasamy, A. (2015): Enhanced visible photocatalytic activity of cotton ball like nano structured Cu doped ZnO for the degradation of organic pollutant, *Ecotoxicology and Environmental Safety* (2015) 132–145
- Vishnukumar, P., Vivekanandhan, S., Misra, M., & Mohanty, A. K. (2018): Recent advances and emerging opportunities in phytochemical synthesis of ZnO nanostructures, *Material Science in Semiconductor processing* 80 (2018) 143-161.
- Wang, D., Jia, F., Wang, H., Chen, F., Fang, Y., Dong, W., & Yuan, X. (2018a). Simultaneously efficient adsorption and photocatalytic degradation of tetracycline by Fe-based MOFs. *Journal of colloid and interface science*, 519, 273-284.
- Wang, J. P., Xu, H., Qian, X. F., Dong, Y. Y., Gao, J. K., Qian, G. D., & Yao, J. M. (2015). Modification of g-C₃N₄ with CuO for enhanced photocatalysis. *Chemistry-Asian Journal*, 10, 1276-1280
- Wang A., Zhang X., Li S., Fang Y., Pan L., & Zou J. J. (2018b). C-doped ZnO ball-in-ball hollow microspheres for efficient photocatalytic and photoelectrochemical applications, *J. Hazard. Mater.* 331 (2018) 235-245

- Wang, J., Chen, R., Xia, Y., Wang, G., Zhao, H., Xiang, L., & Komarneni, S. (2017). Cost-effective large-scale synthesis of oxygen-defective ZnO photocatalyst with superior activities under UV and visible light. *Ceramics International*, *43*(2), 1870-1879.
- Xiong, W., Zeng, G., Yang, Z., Zhou, Y., Zhang, C., Cheng, M., & Li, X. (2018). Adsorption of tetracycline antibiotics from aqueous solutions on nanocomposite multi-walled carbon nanotube functionalized MIL-53 (Fe) as new adsorbent. *Science of the Total Environment*, *627*, 235-244.
- Yasmina, M., Mourad, K., Mohammed, S. H., & Khaoula, C. (2014). Treatment heterogeneous photocatalysis; factors influencing the photocatalytic degradation by TiO₂. *Energy Procedia*, *50*, 559-566.
- Ye, J., Li, X., Hong, J., Chen, J., & Fan, Q. (2015). Photocatalytic degradation of phenol over ZnO nanosheets immobilized on montmorillonite. *Materials Science in Semiconductor Processing*, *39*, 17-22.
- Zhang, L., Zhu, X., Wang, Z., Yun, S., Guo, T., Zhang, J., & Chen, J. (2019). Synthesis of ZnO doped high valence S element and study of photogenerated charges properties. *RSC advances*, *9*(8), 4422-4427.
- Zhu, H., Chen, T., Liu, J., & Li, D. (2018). Adsorption of tetracycline antibiotics from an aqueous solution onto graphene oxide/calcium alginate composite fibers. *RSC advances*, *8*(5), 2616-2621.
- Zhu, X., Pathakoti, K., & Hwang, H. M. (2019). Green synthesis of titanium dioxide and zinc oxide nanoparticles and their usage for antimicrobial applications and environmental remediation. In *Green Synthesis, Characterization and Applications of Nanoparticles* (pp. 223-263).